Archives of Toxicology (2019) 93:887–907
https://doi.org/10.1007/s00204-019-02411-y

NANOTOXICOLOGY

Carbon nanotubes and crystalline silica stimulate robust ROS production, inflammasome activation, and IL-1β secretion in macrophages to induce myofibroblast transformation

Bridget Hindman[1] · **Qiang Ma**[1]

Received: 11 December 2018 / Accepted: 21 January 2019 / Published online: 7 March 2019
© Springer-Verlag GmbH Germany, part of Springer Nature 2019

Abstract
Pulmonary exposure to inhaled particulates elicits complex inflammatory and fibrotic responses that may progress to chronic fibrosis. The fibrogenic potentials of respirable particulates are influenced by their physicochemical properties and their interactions with major pathways to drive fibrotic development in the lung. Macrophages were exposed to six carbon nanotubes (CNTs) of varying dimensions, crystalline silica, or carbon black (CB), with lipopolysaccharide (LPS) and transforming growth factor (TGF)-β1 as positive controls. Macrophage-conditioned media was collected and applied to cultures of human pulmonary fibroblast line WI38-VA13 to induce myofibroblast transformation. Multi-walled and single-walled CNTs (MWCNTs and SWCNTs, respectively) and silica, but not CB, stimulated robust myofibroblast transformation through macrophage-conditioned media. On an equal weight basis, MWCNTs induced higher induction than SWCNTs. High induction was observed for MWCNTs with a long and slender or a short and rigid shape, and silica, at levels comparable to those by LPS and TGF-β1. Fibrogenic particulates induced high levels of IL-1β mRNA expression and protein secretion that are required for macrophage-guided myofibroblast transformation. Induction of IL-1β is dependent on the activation of the NLRP3 (NOD-like receptor family, pyrin domain containing 3) inflammasome and ROS (reactive oxygen species) production in macrophages, as inhibition of NLRP3 by MCC950 and reduction of ROS production by N-acetylcysteine blocked NLRP3 activation, IL-1β induction, and fibroblast activation and differentiation. Therefore, fibrogenic CNTs and silica, but not CB, elicit robust macrophage-guided myofibroblast transformation, which depends on the induction of IL-1β through the NLRP3 inflammasome pathway and the increased production of ROS in macrophages.

Keywords Carbon nanotube · Silica · IL-1β · NLRP3 inflammasome · ROS · Macrophage · Myofibroblast

Introduction

Pulmonary exposure to respirable fibrogenic particles and fibers including certain nanomaterials elicits complex inflammatory and fibrotic responses in the respiratory system that can develop into chronic fibrosis and malignancy in the lung and the pleural space (Donaldson and Seaton 2012; Dong and Ma 2018b; Wynn and Ramalingam 2012). The health outcome of such illness is often devastating, as these diseases are frequently progressive and irreversible once they reach a certain stage, exemplified by pneumoconiosis, lung cancer, and mesothelioma (Donaldson and Seaton 2012; Morgan and Seaton 1995; NIOSH 2002). The mechanism underlying the pathologic development of pulmonary fibrosis and cancer induced by particles and fibers remains undefined, in particular, at the cellular and molecular levels. In part, this contributes to the lack of effective drug therapy that would stop or deter the progression of fibrosis and tumorigenesis in the lung caused by fibrogenic particulate exposure.

At a fundamental level, pulmonary fibrosis resembles overactive wound healing (Dong and Ma 2016b; Duffield et al. 2013). In this context, the normal tissue repair process becomes dysregulated and progressive, leading to continued collagenous matrix deposition and scar formation, and ultimately, respiratory failure. This pathologic tissue repair is

✉ Qiang Ma
qam1@cdc.gov

[1] Receptor Biology Laboratory, Toxicology and Molecular Biology Branch, Health Effects Laboratory Division, National Institute for Occupational Safety and Health, Centers for Disease Control and Prevention, Morgantown, WV 26505, USA

characterized by the persistent activation and functioning of myofibroblasts, which differentiate from resident and migrating fibroblasts (and possibly several other types of cells) and are responsible for continued collagen production and matrix contraction during fibrosis development. Presumably, an assiduous or repetitive tissue injury or, in the case of particulate exposure, prolonged deposition and accumulation of foreign bodies, stimulate the generation of fibrogenic signals that propel the transformation of fibroblasts to myofibroblasts continuously and maintain the cells in an activated state without undergoing apoptosis in fibrosing tissues (Hinz et al. 2012; Tomasek et al. 2002). Given the complexity and dynamics of the cellular and molecular interactions involved in organ fibrosis, such fibrogenic signals would consist of multiple chemical, biological, and physical factors that are specific for inducers and developmental stages of fibrosis, including the initiation, amplification, and chronic progression of organ fibrosis.

Pulmonary macrophages, including alveolar, interstitial, and airway macrophages, arguably constitute the first line of defense against inhaled particulates. These cells are specialized for the clearance of inhaled particles from the lung. Upon encountering particles, macrophages engulf and destroy the particulates by way of degradation. Macrophages also migrate and transport particles to conducting airways and draining lymph nodes for clearance via the airway cilia mucosal system and the lymph-blood circulation, respectively. Additionally, activated macrophages are pivotal in eliciting the inflammatory response to particulates. In this context, macrophages secrete an array of cytokines, chemokines, and growth factors that recruit inflammatory and immune cells and induce the migration, proliferation, and differentiation of fibroblasts. Both the inflammatory and the fibroblast responses are recognized as major events in fibrotic development induced by particulate exposure, highlighting a critical role of the interplay between macrophages and fibroblasts in pulmonary fibrosis (Dong and Ma 2018a, b; Murray and Wynn 2011). Major factors that are derived from macrophages and drive fibrosis development in lungs exposed to particulates remain to be defined, with regard to their specificity, regulation, and mechanism of action.

Among fibrogenic particulates, crystalline silica is a known, potent inducer of fibrosis and tumorigenesis in human lungs, while carbon nanotubes (CNTs) represent new and emerging nanomaterials that exhibit a propensity to cause such lesions. CNTs are respirable and have a fiber-like shape with a high aspect ratio, large surface area, low solubility, and substantial bio-persistence. These properties are often associated with the fibrogenic and tumorigenic effects of inhaled particles and fibers (Donaldson et al. 2006). In fact, pulmonary exposure to certain CNTs causes fibrotic lesions and cancer in the lung and the pleural space in laboratory animals (Dong and Ma 2015; Dong et al. 2015; Mercer et al. 2013; Porter et al. 2010; Sargent et al. 2014; Shvedova et al. 2005; Suzui et al. 2016), raising health concern for exposed workers and consumers. From an occupational and public health perspective, understanding the interrelations between the physicochemical properties of CNTs and their pulmonary effects is critical for the risk assessment and safe design of CNTs and CNT-containing materials. Such understanding would require comparative analyses of CNTs with varying dimensions and properties in relation to their pulmonary effects, in particular, their interactions with the major pathways and events that drive the development of fibrosis and cancer in the lung.

We have previously shown that CNTs elicit a biphasic response in lungs. The early phase response is characterized by acute inflammatory infiltration and cytokine secretion, accompanied by rapid-onset deposition of collagen fibers and accumulation of myofibroblasts near CNT deposits, resulting in the formation of prominent inflammatory fibrotic foci in the lung (Dong and Ma 2016b; Dong et al. 2015). The acute lesions are resolved within 2 weeks post-exposure to a large extent, but not completely. Instead, the fibrotic lesions convert to chronic interstitial fibrosis and granulomas, which last 56 days to a year post-exposure. Notably, a T helper 2 (Th2)-driven type 2 inflammation becomes prominent at the peak of the early phase response and promote the resolution of the acute inflammation and the chronic progression of fibrosis (Dong and Ma 2016a). Consistent with this notion, macrophages in the lungs exhibit an M2 (alternatively activated) phenotype during the type 2 inflammation and mediate many of the type 2 functions, such as the secretion and activation of transforming growth factor (TGF)-β1. The Th2-generated type 2 cytokines interleukin (IL)-4 and IL-13 and M2-generated TGF-β1 are believed to play important roles in promoting the acute-to-chronic transition in lung fibrosis induced by CNTs (Dong and Ma 2018a). During the early acute phase, i.e., prior to type 2 inflammation, pulmonary macrophages manifest an M1 (traditionally activated) phenotype that is implicated in particle phagocytosis and secretion of acute cytokines and chemokines, such as tumor necrosis factor (TNF)-α, IL-1α, IL-1β, and IL-6, by the macrophages. These findings suggest that pulmonary macrophages initiate fibrotic development in the lung by stimulating myofibroblast transformation via soluble fibrogenic cytokines and growth factors in a time- and context-dependent manner (Dong and Ma 2018b). This macrophage–fibroblast interaction through secreted soluble factors may be investigated using conditioned media transfer (He et al. 2011) and pharmacological, immunological, or genetic blockade of cytokine signaling (Dong and Ma 2016c, 2017a, b).

In this study, we compared the fibrogenic potentials among six CNTs of varying dimensions, as well as respirable crystalline silica particles and amorphous carbon black (CB)

nano-particles, in a macrophage-conditioned media transfer model of myofibroblast transformation. This model system enables the investigation of not only the relationship between dimensions and fibrogenic potentials of the particulates, but also the major mediators and signaling mechanisms involved in macrophage-guided myofibroblast transformation and activation. The study reveals that all CNTs tested and silica, but not CB, stimulated robust myofibroblast differentiation and proliferation through macrophage-conditioned media. Higher induction was observed in samples treated with multi-walled CNTs (MWCNTs) with either the largest or the smallest aspect ratio, i.e., MWCNTs with a long and slender or a short and rigid shape, respectively, or samples treated with silica. Induction by these particulates was comparable to induction by lipopolysaccharide (LPS) and TGF-β1, positive controls known to have strong fibrogenic activities. Single-walled CNTs (SWCNTs) induced lower responses than MWCNTs. Mechanistically, IL-1β was identified as a major factor released from activated macrophages to drive the transformation and activation of myofibroblasts in this media transfer model. Moreover, CNTs and silica stimulated robust activation of the NOD-like receptor family, pyrin domain containing 3 (NLRP3) inflammasome, leading to markedly increased production and secretion of IL-1β. Lastly, both NLRP3 activation and IL-1β induction by particulate inducers were strongly inhibited by reactive oxygen species (ROS) scavenger N-acetylcysteine (NAC). Given the controversial and sometimes contradictory literature on the role of IL-1β in organ fibrosis and myofibroblast transformation (Borthwick 2016; Mia et al. 2014; Vesey et al. 2002), this paper adds to our understanding of myofibroblast activation and the fibrotic response to particulates, establishing that fibrogenic particulates stimulate NLRP3 inflammasome activation to increase the production and secretion of IL-1β, which in turn induces the differentiation of fibroblasts into myofibroblasts. Moreover, an induced production of ROS is likely to play an important role in this process. This study thus reveals new insights into the mediators and pathways that drive the early fibrotic response to exposure to CNTs and silica in the lung.

Materials and methods

Source, characterization, and dispersion of CNTs, silica, and CB

Six CNTs of varying physical properties were obtained and given labels based on their relative physical dimensions. Long and slender (M-LS), intermediate (M-IM), and short and slender (M-SS) MWCNTs were purchased from Sigma Aldrich (St. Louis, MO, USA). Short and rigid (M-SR) MWCNTs, i.e., XNRI MWNT-7, were from Mitsui & Company (Tokyo, Japan), and their physical dimensions were classified based on previous reports (Porter et al. 2010). SWCNTs were purchased from Sigma Aldrich and were classified as either long (S-L) or short (S-S) in length.

Major physicochemical properties of the CNTs are summarized in Table 1. M-LS have an average diameter of 12 nm, an average length of 10 µm, a specific surface area of 200 m^2/g, and a metal content of < 2%. M-IM have an average diameter of 10 nm, an average length of 3–6 µm, a specific surface area of 280–350 m^2/g, and a metal content of < 2%. M-SS have an average diameter of 9.5 nm, an average length of 1 µm, a specific surface area of 300 m^2/g, and a metal content of < 5%. M-SR have an average diameter of 49 nm, an average length of 3.68 µm (Porter et al. 2010), a specific surface area of 22 m^2/g (Birch et al. 2013), and

Table 1 Source and physicochemical properties of particulate inducers

Particulates	Label	Source	Dimension	Carbon content	Metal impurity	Iron content	Aspect ratio	Specific surface area (m^2/g)
MWCNTs	M-LS	Sigma (698,849)	12 nm × 10 µm	> 98%	< 2%	–	830	220
	M-IM	Sigma (773,840)	10 nm × 3–6 µm	> 98%	< 2%	–	350–550	280–350
	M-SS	Sigma (755,117)	9.5 nm × 1 µm	> 95%	< 5%	–	105	300
	M-SR	Mitsui (MWNT-7)	49 nm × 3.86 µm	> 95%	< 1%	0.32%	80	22
SWCNTs	S-L	Sigma (704,121)	0.7–1.1 nm × 0.3–2.3 µm	> 90%	< 8%	–	800	700
	S-S	Sigma (652,512)	1–2 nm × 0.5–2 µm	> 90%	< 8%	–	1000	480
Silica	Silica	US Silica (Min-U-Sil 5)	97% < 5 µm in diameter; median diameter 1.6 µm	SiO_2 99.2%	–	Fe_2O_3 0.035%	–	–
Carbon black	CB	Degussa-Heuls (Printex 90)	Average diameter 14 nm	99%	N 0.82% H 0.01%			

Listed physicochemical properties of CNTs used in this study were obtained from the suppliers

a metal content of < 1%. For SWCNT samples used, S-L have a diameter of 0.7–1.1 nm, a length of 0.3–2.3 µm, and a specific surface area of 700 m^2/g (Teran 2016), whereas S-S have a diameter of 1–2 nm, a length of 0.5–2 mm, and a specific surface area of 480 m^2/g; both SWCNTs have metal contents of < 8%. The aspect ratios were substantially higher for the SWCNTs, as well as M-LS, followed by M-IM and M-SS, and lastly by M-SR.

The appearance of CNT fibers in solution was assessed using transmission electron microscopy and images were shown previously (Hindman and Ma 2018). M-LS had a relatively long and slender appearance, with some single fiber tangles or fiber aggregates observed. M-IM appeared to have more variability in length. M-SS were likely to form aggregates; in some cases, fibers were wrapped around each other, forming a rope-like structure. M-SR were visibly thicker and thus more rigid than the other MWCNTs. Additionally, few individual fiber tangles or fiber aggregates were observed for M-SR. Both S-L and S-S formed rope-like structures as described for M-SS fibers, even at high dilutions and with increased sonication.

Crystalline silica (Min-U-Sil® 5) was from U.S. Silica, Berkeley Springs, WV, USA. CB (Printex® 90) was from Degussa-Heuls, Frankfurt, Germany. Respirable crystalline silica particles are known to potently induce pulmonary fibrosis in exposed human and animal lungs, whereas CB induces a pulmonary fibrotic response in animal lungs only at a high dose and is therefore considered as an amorphous, carbonaceous, nano-size particle material with low solubility and low toxicity (Dong et al. 2016; Sager and Castranova 2009). The MIN-U-SIL® 5 silica has 97% of the particles with a length of < 5 µm and a median diameter of 1.6 µm. The specific density of the particles is 2.65 and their content for silicon dioxide (SiO_2) is 99.2% and their content for iron oxide (Fe_2O_3) 0.035%. The Printex 90 particles have an average size of 14 nm and a specific surface area of 295–338 m^2/gm corresponding to a theoretical average spherical particle size of 8.1–9.5 nm. The total carbon content was measured greater than 99% with nitrogen at 0.82% and hydrogen at 0.01%. The organic impurity is less than 1%. The Printex 90 particles in suspension showed an average zeta-size of 140 nm and the hydrodynamic number size distribution of the major mode at 50–60 nm (Jacobsen et al. 2011). Major properties of silica and CB particles are also listed in Table 1.

Stock solutions of particulate inducers were generated by dispersion in culture media with 1% fetal calf serum (FCS) at a concentration of 2 mg/mL by sonication as described previously (He et al. 2011). Stock solutions were further diluted with the culture media and sonicated immediately before use. Vehicle control (VC) samples were treated with an equal amount of the dispersion medium (media with 1% FCS) to establish a baseline response and to validate that there was no effect on the cells from the dispersion medium. The dispersion medium used for VC was sonicated in parallel to preparations of particulate inducers before use.

Cell culture

The murine macrophage line J774A.1 and human pulmonary fibroblast line WI38-VA13 were acquired from ATCC (Manassas, VA, USA). Cells were maintained in Dulbecco's modified Eagle's medium and minimum essential medium-α, respectively, supplemented with 10% FCS, and 1X antibiotic–antimycotic (ThermoFisher Scientific, Waltham, MA, USA). Cultures were maintained at 37 °C in a humidified 5% CO_2 incubator.

Conditioned media and myofibroblast transformation

Macrophages were treated with CNTs (2.5 µg/mL), LPS (2 µg/mL), or TGF-β1 (5 ng/mL) for 24 h at 37 °C. Under these conditions, the cells were as healthy as VC-treated cells with no apparent cytotoxicity. Conditioned media from treated macrophages was then collected and centrifuged at 16,000×*g* for 10 min to remove cellular debris and CNTs, mixed 1:1 with fresh culture media, and applied to WI38-VA13 fibroblasts (He et al. 2011). After incubation in conditioned media for 24 h at 37 °C, fibroblasts were investigated for the expression of α-smooth muscle actin (α-SMA) and proliferation via cell cycle analysis. The effect of IL-1β on fibroblast proliferation and α-SMA expression was also tested by directly treating fibroblasts with 2.5, 5, 10, or 20 ng/mL IL-1β (Sigma-Aldrich). Cell cycle analysis and α-SMA expression were determined using flow cytometry as described previously (Pozarowski and Darzynkiewicz 2004). Briefly, fibroblasts were trypsinized, centrifuged at 300×*g* for 10 min, fixed in cold 0.1% formaldehyde and permeabilized in 0.5% Tween 20 (v/v in PBS). Cells were then washed three times in cold PBS, centrifuged, and incubated in a 1:500 dilution of a monoclonal anti-α-SMA antibody (Sigma Aldrich) with 5 µg/mL Hoescht 33342 dye (Sigma Aldrich) in permeabilization buffer. Cells were then thoroughly washed in PBS and incubated with Alexa 488 goat-anti-mouse antibody (ThermoFisher) before being resuspended in 1% formaldehyde and analyzed using a LSRII Flow Cytometer (BD Sciences, San Jose, CA, USA). Analysis of α-SMA expression and DNA content was performed using Flowing Software (Version 2.5.1, Perttu Terho, Turku Center for Biotechnology, Turku, Finland).

Expression of α-SMA in conditioned media-treated fibroblasts was also examined using immunofluorescent staining. Cells were seeded on glass coverslips and treated as described. After 48-h incubations, cells were fixed in 4% formaldehyde, permeabilized in 0.5% Triton X-100 (v/v

in PBS), blocked in 5% goat serum (v/v in PBS, Sigma Aldrich) and stained for α-SMA actin and F-actin using TRITC-Phalloidin (Sigma Aldrich). Primary antibodies were used at a dilution of 1:500 in 10% blocking buffer (v/v in PBS) overnight at 4 °C. Samples were then washed, incubated in Alexa 488 goat-anti-mouse secondary (1:2000 dilution) for 1 h at room temperature before being mounted in the photobleach resistant mounting media containing DAPI Vectashield (Vector Labs, Burlingame, California, USA). Cells were then imaged using a Zeiss 780 confocal microscope with a Plan-Apochromat 63x/1.40 Oil DIC M27 objective. The full depth of the cell monolayer was imaged at a z-step of 0.5 µm. The average cellular α-SMA content was analyzed (expressed as relative fluorescence units or RFU) using Image J software (Version 1.5.1 g, NIH, Bethesda, MD, USA) and at least 30 cells per treatment were analyzed.

IL-1β ELISA

Macrophages were treated with CNTs (2.5 µg/mL), LPS (2 µg/mL), or TGF-β1 (5 ng/mL) for 24 h followed by 1 h incubation with 5 mM ATP at 37 °C. Cell supernatant was collected and stored at − 80 °C until use. The amount of IL-1β in the supernatant was determined using a mouse ELISA kit (eBioscience, San Diego, California, USA) according to manufacturer's instructions.

Real-time PCR

Macrophages were treated and stimulated with ATP as described. Total cell RNA was isolated using Qiagen RNA mini Kit (Qiagen, Germantown, Maryland, USA) according to manufacturer's instructions. After isolation, 5 µg of total RNA was reverse transcribed using Quantitect Reverse Transcription kit (Qiagen) according to manufacturer's instructions. IL-1β cDNA was amplified and quantified with gene-specific primers by real-time PCR using RT^2 SYBR Green Mastermix (Qiagen) and Applied Biosystems 7300 Real-Time PCR System (ThermoFisher Scientific). Fold change calculations were performed using the Pfaffl method (Fraga et al. 2008).

Evaluation of ASC speck formation by flow cytometry

Macrophages were treated and the NLRP3 inflammasome stimulated as described above. After ATP stimulation, macrophages were harvested by centrifugation and the formation of ASC (apoptosis-associated speck-like protein containing a C-terminal caspase recruitment domain) specks investigated by flow cytometry as described previously (Sester et al. 2016). Briefly, cells were fixed in ethanol and stained for ASC using a 1:1000 dilution of primary antibody (Santa Cruz) overnight at 4 °C. Cells were then incubated in Alexa 488 goat-anti-mouse secondary antibody for 45 min at room temperature before being analyzed using an LSRII flow cytometer (BD Sciences, San Jose, CA, USA). Formation of ASC-containing specks was determined by analyzing the relative peak width and area of the 488 channel. Once activated, cells with an ASC-containing speck exhibit a peak of relatively large height and small width, allowing for quantification of the percentage of cells with activated inflammasomes.

Western blot analysis

J774A.1 cells were investigated for expression of caspase-1 protein via immunoblotting as previously described (He et al. 2011). Briefly, J774A.1 cells were seeded at a density of 70% and were allowed to adhere overnight in a CO_2 incubator at 37 °C. Cells were then treated with 2 µg/mL LPS (Sigma Aldrich), 5 ng/mL TGF-β1 (Sigma Aldrich), or 2.5 µg/mL nanoparticles for 24 hours, followed by 5 mM ATP (Sigma Aldrich) for 1 h at 37 °C to stimulate NLRP3 inflammasome activity. Cells were harvested in cold radioimmune precipitation assay (RIPA) buffer for 30 min, followed by brief sonication and centrifugation to remove cell debris. Protein concentration of cell lysates was determined using a BCA Protein Assay Kit (Bio-Rad, Hercules, California, USA) and equal amounts of protein were loaded onto a 10% SDS–PAGE gel. Samples were transferred to a PVDF membrane (Bio-Rad), blocked with 5% milk in PBST and probed overnight with shaking at 4 °C using a rabbit anti-caspase 1 antibody (Abcam, Cambridge, Massachusetts, USA), followed by an HRP-conjugated anti-rabbit secondary antibody (Bio-Rad). Membranes were developed using enhanced chemiluminescent detection reagents (Fisher Scientific, Pittsburgh, Pennsylvania, USA). β-actin was used as a loading control.

Co-immunoprecipitation

Co-immunoprecipitation of NLRP3 inflammasome components was performed as describe previously (Khare et al. 2016). Briefly, macrophages were treated with vehicle control, LPS (2 µg/mL), M-LS (2.5 µg/ML) or M-SR (2.5 µg/mL) for 24 h in duplicate. One duplicate from each treatment group was also treated with MCC-950. After treatment and ATP stimulation, cells were washed and lysed in ice-cold lysis buffer for 30 min on ice. Lysates were then cleared of cell debris by centrifugation at 16,000×*g* for 15 min at 4 °C, and an aliquot set aside for western blot analysis of total protein input. Lysates were then incubated with 1 µg of anti-ASC antibody (Santa Cruz Biotechnology, Dallas, Texas, USA) for 1 h at room temperature with

rotation before adding protein G-Sepharose beads for overnight incubation with rotation at 4 °C. Immunoprecipitated proteins were extracted from beads with addition of Laemmli buffer and incubation at 95 °C. Sepharose beads were pelleted using centrifugation and cleared samples were run on SDS-PAGE gel for western blot analysis. For western blot analysis of total protein input, equal amounts of protein from cell lysates prior to immunoprecipitation were run on SDS-PAGE gel. PVDF membranes were blocked with 5% milk in PBST and probed with anti-ASC (Santa Cruz Biotechnology) or anti-NLRP3 (Cell Signaling Technology, Danvers, Massachusetts, USA) antibody overnight at 4 °C. Appropriate goat-anti-mouse or goat-anti-rabbit HRP-conjugated secondary antibodies (Bio-Rad) were used and membranes were developed in ECL substrate (Fisher Scientific). β-actin was used as a loading control.

Caspase-1 activity

Macrophages were treated with CNTs (2.5 µg/mL), LPS (2 µg/mL), or TGF-β1 (5 ng/mL) for 24 h followed by 1 h incubation with 5 mM ATP at 37 °C. Cells were collected, centrifuged and lysed for immediate use. Caspase-1 activity was measured using a colorimetric assay according to the manufacturer's instructions (R&D Systems, Minneapolis, Minnesota, USA). Samples containing no cell lysate or no substrate were included as negative controls.

Inhibitor studies

N-Acetyl cysteine (Sigma Aldrich, NAC) was used to block the effect of reactive oxygen species (ROS) on inflammasome activation. Cells were pre-treated with 5 mM NAC for 30 min at 37 °C prior to treatment with fibrotic inducers, and levels of NAC were maintained throughout the 24 h inducer treatment period before secondary stimulation with 5 mM ATP. Cells and conditioned media were then analyzed as described for IL-1β secretion, caspase-1 activity, and activation and proliferative effects on fibroblasts. NLRP3 inflammasome inhibition was achieved using the small molecule inhibitor MCC-950 (Focus Biomolecules, Plymouth Meeting, Pennsylvania, USA) (Coll et al. 2015). After 24-h treatment with fibrotic inducers as described above, macrophages were treated with 1 µM of MCC-950 for 1 hour before secondary stimulation with 5 mM ATP at 37 °C. Cells and conditioned media were then analyzed as described above. In separate experiments, Il-1β was blocked using a neutralizing antibody (Abcam) after fibrotic inducer treatment and ATP stimulation.

Detection of ROS

Macrophages were seeded onto glass coverslips and allowed to adhere for 24 h in a CO_2 incubator at 37 °C before treatment with inducers and ATP stimulation as described above. The relative ROS levels within treated cells was evaluated using dihydroethidium (DHE) staining as described previously (He and Ma 2012). Briefly, 30 mins before the end of ATP stimulation, DHE (ThermoFisher Scientific) was added at a concentration of 5 mM. Cells were then fixed in formaldehyde, mounted in Vectashield, and imaged using a Zeiss 780 confocal microscope with a Plan-Apochromat 20 ×/0.8 M27 objective. Relative DHE fluorescence was analyzed using Image J software and is represented as the mean and SD of five separate fields for each treatment.

Statistical analysis

Statistical analysis was performed using GraphPad Prism software (Version 7.02, GraphPad Software Inc., La Jolla, CA, USA). All experiments were performed in triplicate and experiments were repeated three times. Data are presented as mean ± SD. Statistical significance was determined using one-way ANOVA followed by a Tukey post-test for between sample comparisons. In most cases, all fibrotic agents resulted in significant changes over vehicle control treated cells; therefore, statistical analyses shown in figures are often comparisons between different particulate inducers (all CNTs, plus CB and silica). $*p < 0.05$; $**p < 0.01$; and $***p < 0.001$.

Results

Conditioned media from macrophages exposed to CNTs of varying dimensions or silica induce myofibroblast transformation in a media transfer model

We have previously developed a conditioned media transfer model in which interactions between two types of cells are manifested through secreted molecules in the media (He et al. 2011). In this study, we used this approach to examine and compare the effects of six CNT fibers of varying dimensions, crystalline silica, and CB nano-particles on the ability of macrophages to stimulate fibroblasts to differentiate into myofibroblasts, a key cellular event during the initiation, amplification, and chronic progression of pulmonary fibrosis. The six CNTs were long and slender (M-LS), intermediate (M-IM), and short and slender (M-SS), short and rigid (M-SR, i.e., XNRI MWNT-7) MWCNTs, and long (S-L) and short (S-S) SWCNTs. Major physicochemical properties of the CNTs, silica, and CB are summarized in Table 1. The

appearance of CNT fibers in solution was assessed using transmission electron microscopy and was shown elsewhere (Hindman and Ma 2018).

As diagramed in Fig. 1a, after treatment with fibrotic inducers, the conditioned media from treated macrophages was applied to fibroblasts, and fibroblasts were examined for α-SMA expression, a commonly used biomarker for myofibroblast differentiation, as well as cell proliferation, which reflects the mitogenic activity of the inducers. Fibroblast α-SMA expression in response to treatment with macrophage-conditioned media was measured by flow cytometry, which detects the α-SMA protein expression in a large population of cells quantitatively with high efficiency. Quantification is presented in the column graph in Fig. 1b.

Fibroblasts with no conditioned media (No CM) or fibroblasts treated with vehicle control-conditioned media (VC) exhibited very low levels of basal α-SMA expression, shown as the percent of cells positive for α-SMA expression at 3.2% and 2.6%, respectively. LPS and TGF-β1 are known to induce α-SMA expression in vivo and in cultured fibroblasts rapidly with high potency and, therefore, were used as positive controls for induced expression of α-SMA. As expected, LPS or TGF-β1-conditioned media stimulated high levels of α-SMA expression, reaching 88.2% and 90% of treated cells, respectively. Fibroblasts incubated with conditioned media from macrophages exposed to CNTs had a majority of the cells expressing α-SMA. Among the samples, 87.5% of fibroblasts incubated with M-LS-conditioned media expressed α-SMA, which was significantly higher than fibroblasts incubated with M-IM or M-SS-conditioned media (73.4% and 78%, respectively). Cells incubated with M-SR-conditioned media had 86.1% of the cells expressing α-SMA and there was no significant difference between M-LS and M-SR sample groups, indicating similar potencies of M-SR and M-LS for α-SMA induction in this media transfer model. The SWCNTs-conditioned media also induced high percentages of α-SMA expressing in fibroblasts, with S-L inducing 72% and S-S inducing 67.7% of the cells to express this protein. However, these inductive activities of SWCNTs were significantly lower than that of M-LS. Therefore, M-LS, which has the largest aspect ratio, and M-SR, which has the smallest aspect ratio, had the highest inductive activities for α-SMA expression among the CNTs tested.

CB is an amorphous, carbonaceous, nano-sized particle material and is an example of low solubility low toxicity particles that cause pulmonary fibrosis in rodents only at a high

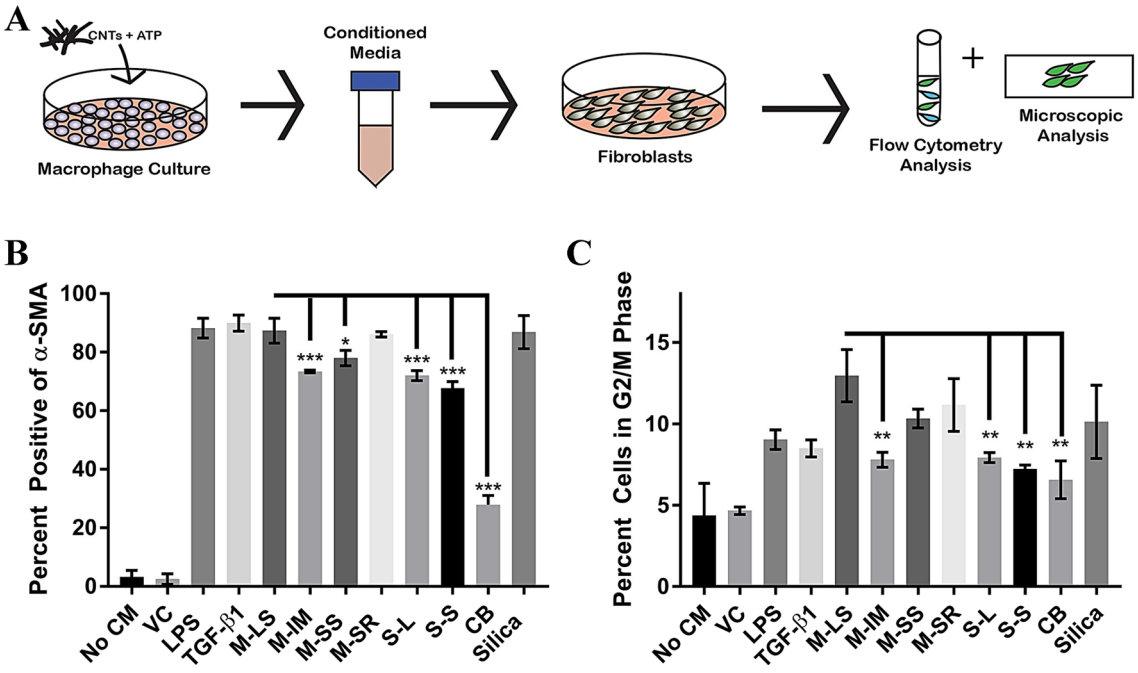

Fig. 1 Conditioned media from macrophages treated with fibrogenic agents induces myofibroblast differentiation and proliferation. **a** A schematic outline of the experimental setup for conditioned media assays. J774A.1 macrophages were treated with 2 μg/mL LPS, 5 ng/mL TGF-β1, or 2.5 μg/mL particulate inducers (CNTs, CB, or silica). No conditioned media (no CM) and treatment with vehicle only (VC) were used as controls. After 24 h, cells were stimulated with 5 mM ATP for 1 h and the conditioned media was collected and applied to WI38-VA13 pulmonary fibroblasts. Fibroblasts were then examined for α-SMA expression (**b**) or proliferation using cell cycle analysis as an indicator (**c**). Conditioned media from macrophages treated with fibrogenic inducers significantly increased α-SMA expression across all treatments over controls (no CM or VC). For cell cycle analysis, all fibrogenic inducers induced significant increase of percent cells in the G2/M phase, except CB, compared with no CM or VC. Statistical comparison between M-LS and each other particulate inducer is shown. *$p < 0.05$; **$p < 0.01$; ***$p < 0.001$

dose. CB induced α-SMA expression in 27.8% of the treated cells, which is significantly higher than No CM or VC, but is substantially lower than those of CNT samples, consistent with its low fibrogenic activity in vivo. On the other hand, crystalline silica induced the expression of α-SMA in 86.9% of treated cells, which is comparable to those by M-LS and M-SR, and is consistent with silica being a potent fibrotic inducer in human and animal lungs.

The mitogenic effects of the CNTs and silica were examined as increased cell proliferation, indicated as elevated relative fractions of cells in the G2/M stage of the cell cycle, i.e., fractions of cells currently undergoing cell division (Fig. 1c). Cell proliferation was analyzed using flow cytometry, staining cells with Hoescht 3342 dye that binds to DNA. Fibroblasts incubated with No CM or VC-conditioned media had 4.4% and 4.7% of cells in the G2/M phase division as basal levels of cell division, respectively. Incubation with LPS or TGF-β1 increased the cells in the G2/M phase to 9.1% and 8.7%, respectively, indicating the cells were undergoing cell division at a greater rate than No CM or VC fibroblasts. Particulate inducers increased the percentage of cells in the G2/M phase of the cell cycle as the following: M-LS to 12.9%; M-IM to 7.8%; M-SS to 10.3%; M-SR to 11.2%; S-L to 7.9%; S-S to 7.2%; CB to 6.6%; and Silica to 10.1%. As with the α-SMA expression data presented above, M-LS had the largest effect among all inducers. This effect was significantly higher than M-IM, S-L, and S-S. The mitogenic effects of M-LS, M-SR, and silica were similar to each other without statistical significance. Because LPS, TGF-β1, and M-LS induced α-SMA expression at similar levels (Fig. 1b), but LPS and TGF-β1 increased cell division at levels that are nearly 40% lower than M-LS (Fig. 1c), these inducers exhibit differential activities on myofibroblast differentiation and proliferation.

A hallmark of myofibroblast differentiation and activation is the incorporation of the newly synthesized α-SMA into contractile stress fibers, which strengthens contraction by myofibroblasts. This feature is unique to activated myofibroblasts and can be examined morphologically by confocal microscopy. Fibroblasts incubated with macrophage-conditioned media were fixed and stained for α-SMA and F-actin to determine if the treatment induced an increase in the appearance of contractile stress fibers as well as the incorporation of α-SMA into such fibers (Fig. 2a). The relative expression of α-SMA was quantified as fluorescence intensity (RFU) (Fig. 2b). Fibroblasts incubated with conditioned media from VC-treated macrophages expressed nearly no detectable level of α-SMA. Fibroblasts incubated with LPS-conditioned media, however, showed a marked increase in the formation of thick, bundled actin fibers consistent with contractile stress fibers, indicated by white arrowhead in the F-actin channel, and these stress fibers contained α-SMA, indicated by cyan arrowhead in the merged

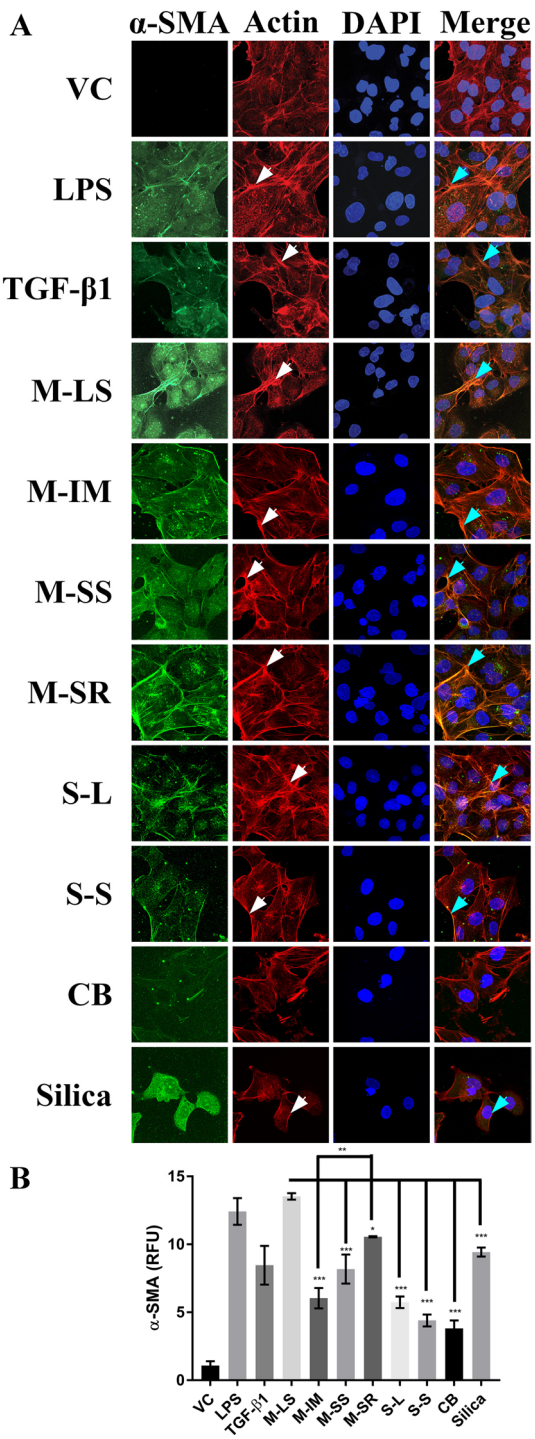

Fig. 2 Macrophage-conditioned media activates fibroblasts to a contractile myofibroblast phenotype. J774A.1 macrophages were treated and their conditioned media harvested as described in Fig. 1 legend. Fibroblasts were then grown in macrophage-conditioned media for 24 h before being stained for α-SMA (green channel), F-actin (red channel), and DAPI (blue channel). **a** Representative images are shown. White arrowheads on the F-actin channel indicate areas containing contractile stress fibers and cyan arrows on the merged images indicate α-SMA localized to stress fibers. **b** α-SMA staining is presented in RFU as means ± SD from three separate experiments. Statistical comparison between M-LS and each other particulate inducer is shown. $^{*}p < 0.05$; $^{**}p < 0.01$; $^{***}p < 0.001$

channel. TGF-β1-treated conditioned media also increased the expression and incorporation of α-SMA into stress fibers, though not to the same extent as LPS. For particulate fibrotic inducers, results were qualitatively similar to those obtained using flow cytometry. While all particulate inducers increased α-SMA expression and its incorporation into stress fibers to some extent, the M-LS treatment had the largest effect, followed by M-SR, M-SS, M-IM, and finally SWCNTs. Silica induced a high level of α-SMA expression and formation of stress fibers, similarly to M-SR, whereas CB had only a very weak, albeit significantly higher than VC, effect.

Taken together, these results indicate that treatment with fibrogenic particulate agents stimulate macrophages to produce soluble factors that activate fibroblasts to differentiate into myofibroblasts. Given that macrophage activation and secretion in this in vitro model mimics the early response of macrophages to inflammatory and fibrogenic inducers in the lung, this finding suggests a potentially important mechanism for the initiation of pulmonary fibrosis. Among the particulate inducers, the M-LS CNTs with a long length and large aspect ratio, M-SR CNTs with a large diameter and small aspect ratio, and crystalline silica in the respirable particle size range exhibited consistently high levels of inducing activities compared with M-IM, M-SS, S-L, and S-S CNTs, whereas the amorphous carbonaceous CB nanoparticles produced the smallest effects above the low basal levels, for myofibroblast transformation and proliferation, in this conditioned media transfer system.

CNTs and silica stimulate macrophages to produce and secrete IL-1β that induce myofibroblast transformation

Macrophages secrete a host of growth factors, cytokines, and chemokines in response to treatment with CNTs (He et al. 2011). Among the soluble factors released from macrophages, TGF-β1 is believed, in conjunction with Th2 cell-produced IL-13 and/or Th17 cell-produced IL-17, to play an important role in promoting fibrotic responses, in particular, during the fibrotic progression to chronic pulmonary fibrosis. On the other hand, cytokines that are acutely produced by activated macrophages may provide an initial signal to stimulate the acute phase fibrotic response in the lung in an exposure, time, and context-dependent manner. This macrophage-guided fibroblast response co-occurs with acute inflammation to lead to the formation of inflammatory and fibrotic foci characteristic of the early stage pathology induced by fibrogenic particulates (Dong and Ma 2018b; Gieseck et al. 2017). Among the early inflammatory cytokines released by macrophages, IL-1β has been shown to exhibit certain fibrogenic activities, albeit its role in particulate-induced lung fibrosis remains a subject of considerable debate. Therefore, we examined IL-1β for further study in an effort to identify a soluble factor(s) responsible for macrophage-guided myofibroblast transformation using the conditioned media transfer model.

We first examined the induced production and secretion of active IL-1β protein from macrophages stimulated by CNTs and silica using an ELISA assay. As expected, LPS or TGF-β1-treated cells secreted IL-1β at high levels, i.e., 365 ng/mL and 310 ng/mL, respectively, which are 5.8- and 4.9-fold higher than VC (63 ng/mL), demonstrating a robust and specific induction of IL-1β by the inducers (Fig. 3a). M-LS-treated cells secreted IL-1β at 381 ng/mL, comparable to LPS-treated cells and significantly greater than all other particulate inducer-treated cells. Cells treated with M-IM secreted IL-1β at 310 ng/mL, with M-SS at 230 ng/mL, and

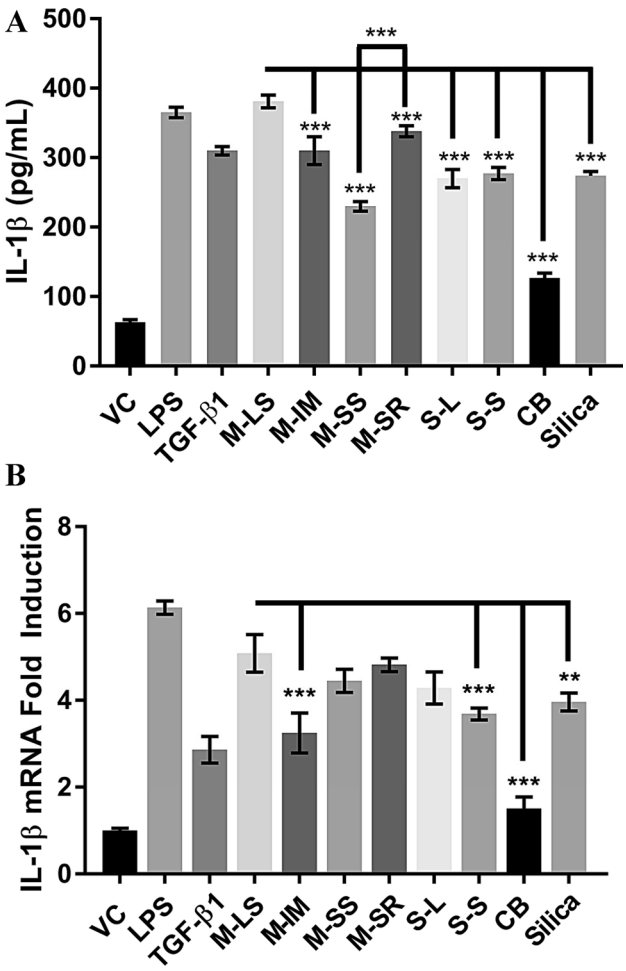

Fig. 3 Macrophages respond to CNT treatment with elevated levels of secreted IL-1β and its mRNA expression. J774A.1 macrophages were treated as described for Fig. 1. After ATP stimulation, the conditioned media and cells were harvested for **a** ELISA or **b** RT-PCR to analyze levels of secreted IL-1β and its mRNA expression, respectively. Treatment with fibrogenic agents or LPS significantly increased the secreted IL-1β level and the IL-1β mRNA expression across all agents. $^{**}p < 0.01$; $^{***}p < 0.001$

with M-SR at 338 ng/mL. The difference between M-SS and M-SR was significantly different. SWCNT-treated cells secreted comparable levels of IL-1β, with S-L cells secreting at 270 ng/mL and S-S cells secreting at 277 ng/mL. Finally, CB-treated cells secreted IL-1β at 127 ng/mL, which is the lowest among CNTs but is significantly higher than VC with a 2.0-fold increase, consistent with its effect as a weak inducer of fibrosis in vivo. Silica-treated cells secreted IL-1β at 274 ng/mL with a 4.4-fold increase over VC, comparable to the increases by most CNTs.

We also examined if the mRNA expression of IL-1β was increased by particulate inducers using quantitative real-time PCR (Fig. 3b). LPS induced a 6.1-fold increase in IL-1β mRNA level in comparison with VC. Cells treated with TGF-β1 had a 2.9-fold increase in mRNA levels, which was markedly lower than that by LPS, revealing differential inductive effects on IL-1β mRNA expression between LPS and TGF-β1. CNT-treated macrophages expressed varied amounts of IL-1β mRNA levels, indicating differences in their potency to increase the expression and/or stability of IL-1β mRNA. Cells treated with M-LS had a 5.1-fold increase, a significantly higher change in mRNA than cells treated with M-IM (3.25-fold increase). The difference between M-LS and the other two MWCNT samples, M-SS (4.45-fold increase) and M-SR (4.8-fold increase) was not statistically significant. SWCNTs also induced IL-1β mRNA to high levels with S-L inducing a 4.3-fold increase and S-S inducing a 3.7-fold increase. Finally, CB induced a 1.5-fold increase, which was not statistically different from VC. Silica induced a 3.97-fold increase similarly to most MWCNTs and SWCNTs. These results indicate CNT fibers and silica particles induce IL-1β mRNA to high levels, which likely contributes to increased levels of IL-1β protein by the inducers.

We then tested if IL-1β induces α-SMA expression when added to the culture media. Figure 4 shows the effect of varying amounts of IL-1β on the morphology and α-SMA expression of fibroblasts. As a positive control, TGF-β1 was shown to induce significant changes in the morphology (Fig. 4a), the percent of α-SMA-positive cells measured by flow cytometry (Fig. 4b), and the relative amount of α-SMA measured by fluorescence intensity (Fig. 4c), compared to VC. IL-1β induced a significant increase in α-SMA expression and its incorporation into stress fibers in a concentration-dependent manner, in a concentration range from 2.5 to 20 ng/mL (Fig. 4a). As measured by flow cytometry, the lowest dose of IL-1β (2.5 ng/mL) induced α-SMA expression in 43.5% of cells, which increased to 62.1%, 85%, and 90% upon increasing concentrations of IL-1β to 5, 10, and 20 ng/mL, respectively (Fig. 4b). Increased expression of α-SMA was also observed to be concentration-dependent, when the relative fluorescence intensity of α-SMA was measured (Fig. 4c). Additionally, IL-1β increased cell proliferation in a concentration-responsive fashion. VC-treated cells had 4.4% in the G2/M phase fraction, which increased to 12.5% of cells in the most responsive IL-1β dose (10 ng/mL). Collectively, the results indicate that IL-1β is induced by CNTs and silica at both protein and mRNA levels and is capable of stimulating myofibroblast differentiation and proliferation directly.

To establish a role of IL-1β in the observed macrophage-guided myofibroblast transformation, we used an antibody against IL-1β to neutralize this cytokine in the conditioned media from macrophages treated with fibrotic inducers. Indeed, conditioned media incubated with the neutralizing antibody had a significantly lower ability to induce fibroblast activation measured by flow cytometry (Fig. 4e) with a reduction of about 50% or more for most CNTs. Interestingly, while the anti-IL-1β antibody blocked the induction by silica by 60%, it did not affect the induced expression of α-SMA by CB. The blocking antibody also reduced fibroblast proliferation (Fig. 4f), but with a smaller effect compared with induction of α-SMA expression (compare Fig. 4e, f). These results indicate that IL-1β indeed plays a major role in the induced macrophage effects on fibroblasts in this conditioned media transfer model.

CNTs and silica stimulate NLRP3 inflammasome activation in macrophages to increase IL-1β production

IL-1β is expressed as inactive pro-IL-1β in cells and is secreted as the active IL-1β after cleavage by caspase-1. This maturation and secretion of IL-1β is dependent upon the activation of the NLRP3 inflammasome in the cytoplasm (Guo et al. 2015). Therefore, we examined the effect of CNTs and silica on NLRP3 inflammasome activation in macrophages.

An early step in NLRP3 inflammasome activation is the association of NLRP3 and ASC, which triggers the oligomerization of the proteins to form a single, speck-like, cytoplasmic, multi-protein complex. We first determined if the treatment induced an increase in the amount of ASC speck formation. Un-activated ASC is expressed in a diffuse cytosolic pattern in cells. Upon activation, ASC binds NLRP3 and coalesces into the NLRP3 inflammasome, forming as a small but very intensely fluorescent cytoplasmic "speck" after anti-ASC immunofluorescence staining. By analyzing the change in the fluorescent peak width versus peak area, cells containing an ASC speck can be identified by flow cytometry, as such cells would exhibit a strong, but narrow, fluorescent peak (Sester et al. 2016). The results for ASC speck formation analyzed using flow cytometry are presented in Fig. 5a. Cells treated with VC had merely 1.9% of cells positive for speck formation, indicating a very low level of NLRP3 inflammasome activation under a basal condition

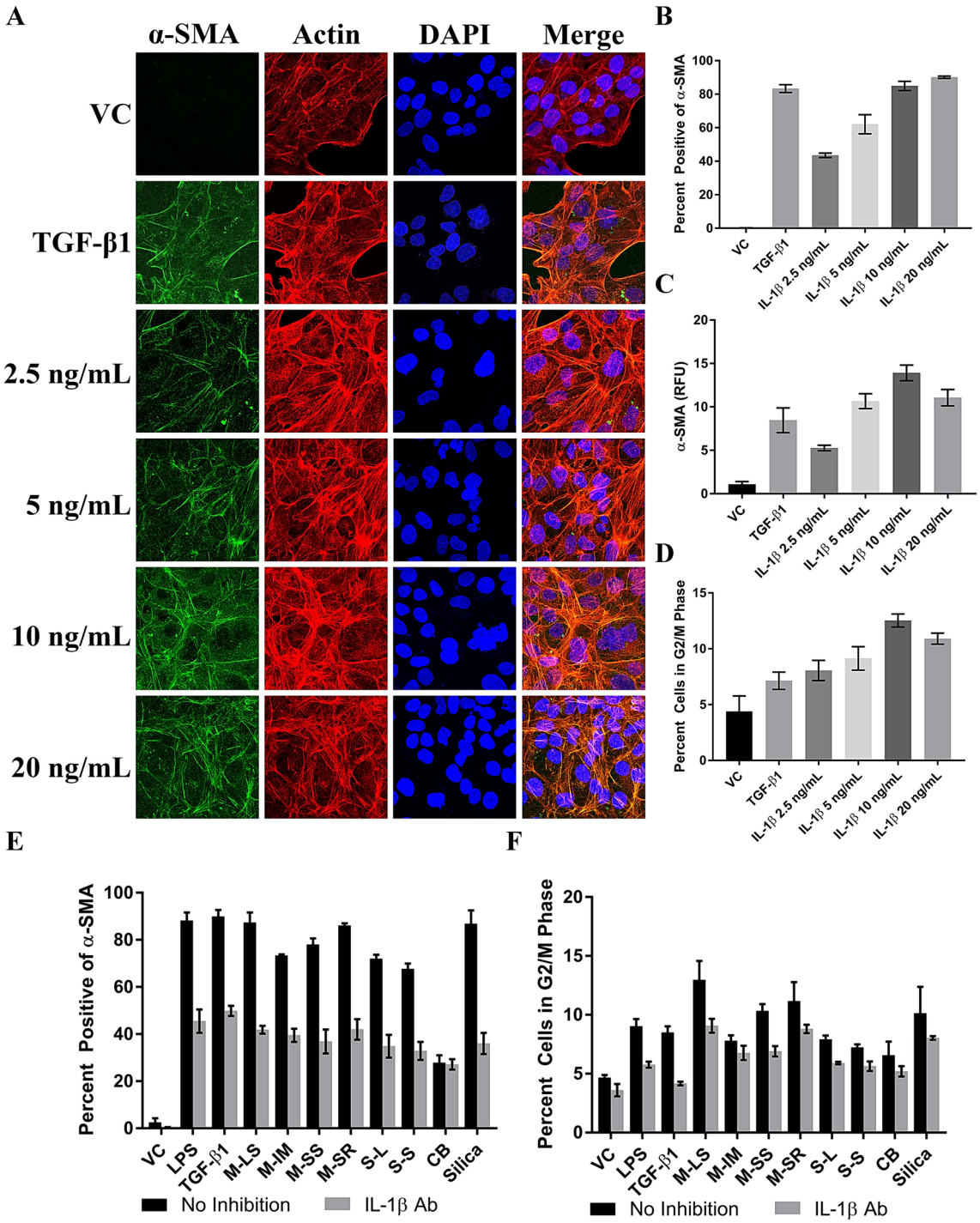

Fig. 4 IL-1β induced myofibroblast differentiation and proliferation. **a** Fibroblasts were treated with TGF-β1 (5 ng/mL), or increasing amounts of IL-1β for 24 h before being examined for α-SMA incorporation into stress fibers, **b, c** expression levels, and **d** proliferation. **e, f** Cells were treated with indicated fibrotic inducers as well as an IL-1β neutralizing antibody and examined for α-SMA expression and cell cycle analysis. Statistical comparisons with VC and between M-LS and each other particulate inducer are discussed in the text

in macrophages. LPS-treated cells were 33.1% positive for speck formation with a 17.4-fold increase, while TGF-β1-treated cells were 30.2% positive with a 15.9-fold increase over VC. The ability to detect a significant increase in cells with positive speck formation upon stimulation with the positive controls for macrophage activation indicates that this method is sensitive and robust. We then expanded to include treatment with the particulate fibrotic agents. Macrophages

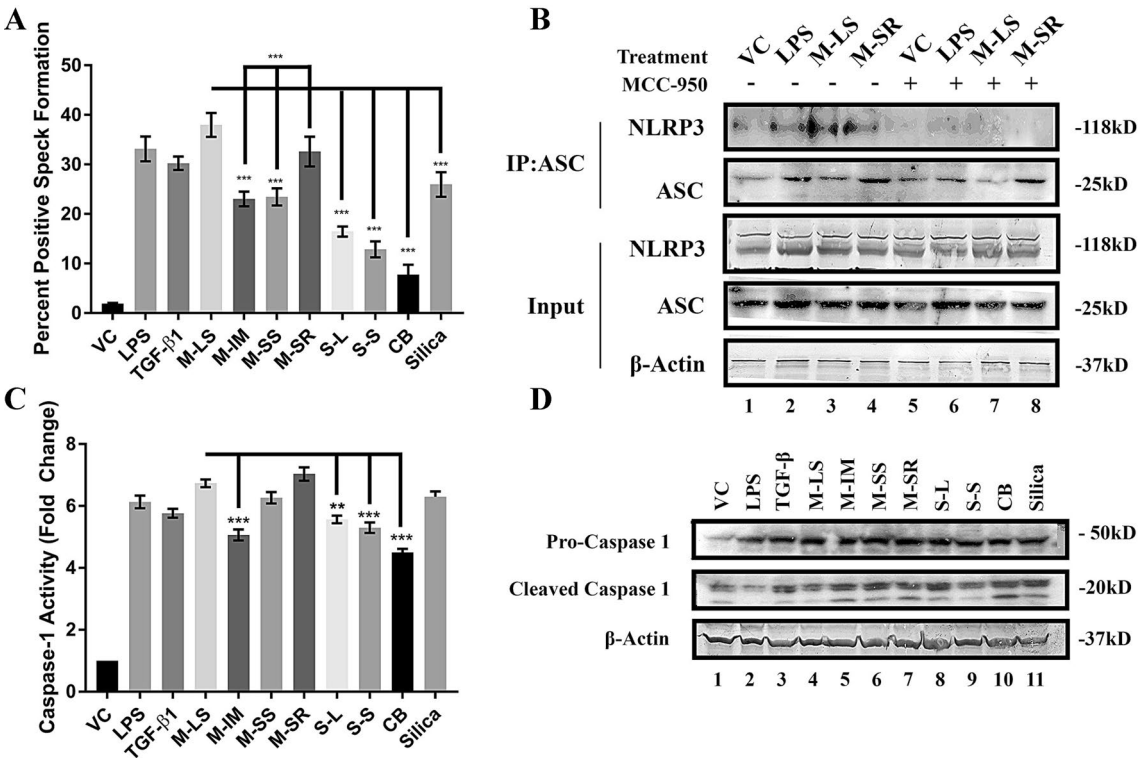

Fig. 5 Fibrotic inducers activate the NLRP3 inflammasome. **a** Macrophages were treated with LPS, TGF-β1, and particulate inducers as indicated. After 24-h treatment, cells were stimulated with ATP and the formation of ASC-containing specks was investigated using flow cytometry. The percentage of cells positive for ASC speck formation was quantified by flow cytometry. **b** Macrophages were treated with vehicle control, 2 μg/mL LPS, 5 ng/mL TGF-β1, or 2.5 μg/mL M-LS or M-SR. After 24 h treatment, cells were stimulated with vehicle control (lanes 1–4) or 1 μM MCC-950 (lanes 5–8), an inflammasome inhibitor, for 1 h followed by ATP stimulation. Cells were then harvested, and co-immunoprecipitation studies completed, using an antibody against ASC. Samples, including immunoprecipitated and total cell lysate, were analyzed using western blot analysis and probed for either NLRP3 (MW 118 kD) or ASC (MW 25 kD), with β-actin (MW 37 kD) as a loading control. All treatment groups induced NLRP3/ASC co-immunoprecipitation, which was blocked by MCC-950 treatment. **c** After stimulation with fibrotic agents, cells were harvested and analyzed for caspase-1 activity using a colorimetric assay. All inducers significantly increased caspase-1 activity over VC. **d** J774A.1 cells were treated as described for Fig. 1. After stimulation, cells were harvested in the RIPA buffer and equal amounts of proteins loaded for western blot analysis of caspase-1. All inducers stimulated expression of pro-caspase-1 (MW 50 kDa), and had varied effects on the amount of cleaved caspase-1 product (MW 20 kDa). β-actin was used as a loading control. $^{**}p < 0.01$; $^{***}p < 0.001$

treated with M-LS, M-IM, M-SS, or M-SR had 38%, 23%, 23.5%, and 32.6% cells positive for speck formation, respectively. SWCNT-treated samples had a significantly smaller percentage of cells form ASC specks at 16.5% (S-L) and 12.9% (S-S) that are significantly higher than VC. While CB induced a 3.9-fold increase, silica induced a 15-fold increase over VC. Therefore, LPS, TGF-β1, M-LS, M-SR, and silica induced inflammasome speck formation to similar high levels. The relative differences among different inducers are consistent with their ability to induce IL-1β secretion, as compared with Fig. 3.

To further validate the induced NLRPS-ASC association, we performed co-immunoprecipitation studies on macrophages treated with selected agents. Cells were treated with vehicle control, LPS, and M-LS or M-SR, the two most potent fibrotic inducers among the panel of CNTs used in this study, and investigated using co-immunoprecipitation with the initial immunoprecipitation performed using an antibody against ASC (Fig. 5b). Treatment with all inducers increased the association of ASC with NLRP3 compared to vehicle control treatment (lanes 1–4, top band). The input panels show that equal amounts of inflammasome components and total protein were probed, indicating that the increase in NLRP3-ASC co-immunoprecipitation was not simply due to an increase in the amount of these proteins in the cells.

Activated ASC associates with pro-caspase-1 leading to its cleavage and the release of activated caspase-1, which cleaves pro-IL1β to IL-1β before IL-1β secretion. We measured caspase-1 activity (Fig. 5c) and the formation of cleaved caspase-1 (Fig. 5d). LPS-treated cells exhibited a 6.1-fold higher caspase activity than VC. TGF-β1-treated cells had a 5.8-fold higher activity than VC. Of the particle inducers, M-LS and M-SR had the largest increase in

caspase activities, i.e., 6.7 and sevenfold higher than that of VC and greater than the caspase activity seen in the other two MWCNT samples, M-IM (5.1-fold) and M-SS (6.3-fold), though only the difference between M-IM and M-LS/M-SR reached statistical significance. S-L or S-S-treated cells exhibited significantly higher activities than VC, at 5.6- and 5.3-fold, respectively, which are nonetheless significantly lower than MWCNT treatments. Finally, CB exhibited the lowest increase in caspase activity (4.3-fold), while silica increased activity to levels comparable to those seen in M-SS treated cells (6.3-fold). These increases qualitatively correlate with the formation of cleaved caspase-1 (MW 20 kDa) from pre-caspase-1 (MW 45 kDa) revealed by immunoblotting (Fig. 5d). These results indicate that treatment with particulate inducers of fibrosis activates NLRP3 inflammasome, as indicated by NLRP3-ASC association, ASC speck formation, and caspase-1 activation.

Having established that CNT treatment activates the NLRP3 inflammasome, we sought to determine how inhibition of the inflammasome would affect inflammasome activation, IL-1β production, and myofibroblast transformation. We chose to use MCC-950, a small molecule that inhibits inflammasome activation by blocking the association between NLRP3 and ASC, thereby inhibiting inflammasome activation, caspase-1 activity, and IL-1β secretion (Coll et al. 2015). We first confirmed that MCC-950 prevents the binding between NLRP3 and ASC by showing that, while LPS, M-LS, and M-SR induced strong co-immunoprecipitation between NLRP3 and ASC, these treatments did not induce detectable co-immunoprecipitation between the two proteins in the presence of MCC950 (Fig. 5b, top band, compare lanes 5–8 with lanes 1–4).

Macrophages treated with fibrotic agents with or without MCC-950 were then examined for the formation of ASC speck, caspase-1 activity, and IL-1β secretion (Fig. 6a–c). For all treatments, MCC-950 decreased the formation of ASC speck by 40–55% (Fig. 6a). Cells treated with MCC-950 also showed a significant decrease in caspase-1 activity, with an average fall of about 30%. The difference between caspase-1 activity levels in uninhibited and MCC-950 treated samples was statistically significant across all groups, except the VC group (Fig. 6b). Similarly to the ASC speck formation and caspase activity levels, IL-1β levels were significantly decreased upon MCC-950 treatment across treatment groups, with a 50–70% decrease for the inducers. These results indicate that MCC-950 treatment largely reduced NLRP3 inflammasome activation and IL-1β secretion.

We determined the functional consequence of inhibition of the NLRP3 inflammasome by MCC-950 using myofibroblast transformation in the conditioned media transfer model as an end point. Macrophages were treated with fibrotic agents, followed by MCC-950 treatment, before the conditioned media was collected and applied to fibroblasts. The fibroblasts were then examined for α-SMA expression and cell proliferation (Fig. 6d–f). Inflammasome inhibition with MCC-950 significantly reduced the expression α-SMA in all treatment groups except for CB, as measured by both flow cytometry (Fig. 6d) and immunofluorescent microscopy (Fig. 6e). Across all fibrotic agent treatment groups, excepting CB, there was a 50–72% decrease in the number of cells positive for α-SMA expression, and the cells that expressed α-SMA had significantly less α-SMA fluorescence intensity in the presence of MCC-950 than treatment groups without MCC-950. MCC-950 co-treatment also decreased the percent cells in G2/M phase, although this effect on cell cycle was not as pronounced as those observed for α-SMA expression, for the majority of treatment groups (Fig. 6f). For conditioned media from MCC-950 treated cells, all treatment groups had a significantly reduced fraction of cells in the G2/M phase of division (Fig. 6f), with decreases from 32% (VC) to 50% (M-SS, M-SR, Silica). Taken together, these results indicate that NLRP3 inflammasome activation is an important mechanism by which CNTs and silica elicit macrophage-guided fibroblast activation and proliferation via the production and secretion of IL-1β.

ROS are driving signals for CNT and silica-induced NLRP3 inflammasome activation in macrophages

The mechanism by which various inducers activate NLRP3 remains largely unclear. In particular, the initial signals elicited by the inducers and upstream of NLRP3-ASC interaction have not been established, which are likely to be inducer and cell context-dependent. One leading candidate is ROS, which have been shown to be increased in activated macrophages in response to a variety of inflammasome agonists (de Zoete et al. 2014; He et al. 2011). Therefore, we investigated if CNTs and silica induce NLRP3 activation by stimulating ROS production.

We first examined and quantified the effect of various CNTs and silica on ROS levels in macrophages, using the fluorescent marker DHE, which fluoresces in the red spectrum in the presence of ROS (Fig. 7). As can be readily seen, treatment with the fibrotic inducers caused a drastic increase in the ROS levels within macrophages. The relative fluorescent intensity of VC-treated cells was 0.5, compared with 9.5 and 13.7 for LPS and TGF-β1, i.e., 19- and 27.4-fold increases, respectively. Treatment with MWCNTs caused an even greater increase in the ROS levels. M-LS had the greatest effect, increasing the DHE fluorescent intensity to 23.7 with a 47.4-fold increase over VC. As with the other assays performed here, M-SR had the next greatest effect on the cells, increasing fluorescent intensity to 19.1 with a 38.2-fold increase. This was followed by M-IM at 16.6 (a 33.2-fold increase) and M-SS at 14.9 (a 29.8-fold increase). SWCNTs had the least effect of all of the CNTs studied,

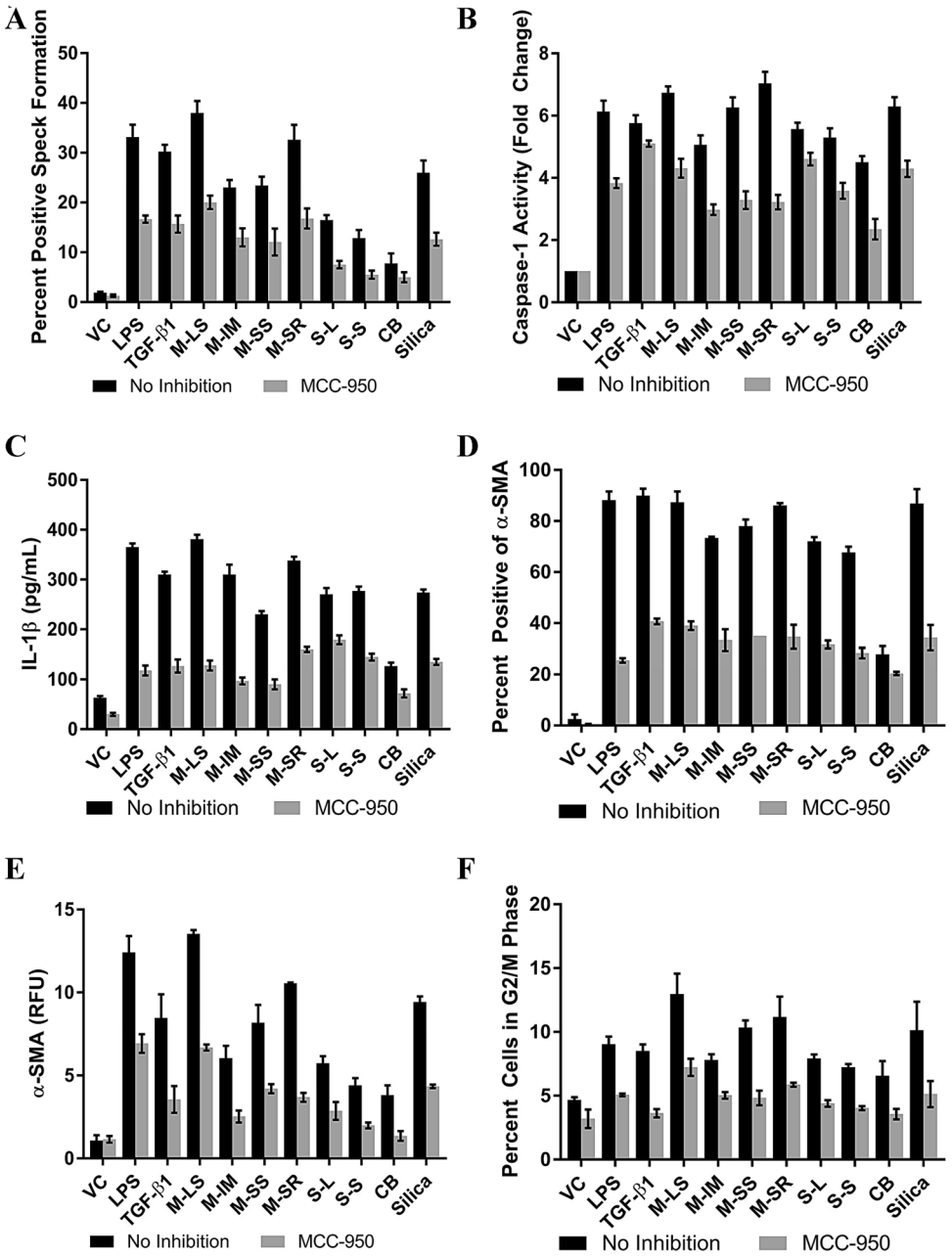

Fig. 6 Inhibition of the NLRP3 inflammasome blocks the effects of macrophage-conditioned media on fibroblasts. J774A.1 macrophages were treated with fibrogenic inducers as described for Fig. 1, and inhibition was achieved with 1 μM MCC-950. Macrophages were examined for ASC speck formation (**a**) caspase-1 activity (**b**) and IL-1β protein secretion (**c**). Inhibition of inflammasome activation significantly reduced ASC speck formation (**a**), caspase-1 activity (**b**), and IL-1β secretion (**c**). Conditioned media from treated macrophages was applied to fibroblasts, and the proliferative and activation effects examined. Inhibition with MCC-950 significantly reduced α-SMA expression (**d, e**) and proliferation (**f**) in treated fibroblasts across all treatment groups, compared with VC, as discussed in the text

with both S-L and S-S increasing DHE fluorescence to 12, a 24-fold increase over VC. Carbon black and silica, which are weak and potent fibrotic inducers, respectively, increased DHE fluorescence to 3 and 16, i.e., 6 and 32-fold increases, accordingly. These results are qualitatively consistent with the results presented above on NLRP3 activation, caspase-1 activity, and IL-1β release.

To examine if the increased ROS levels observed with these fibrogenic agents are involved in the activation of the NLRP3 inflammasome, we used the ROS scavenger NAC. Cells were treated with fibrotic inducers in the absence or presence of NAC, and the effect of NAC co-treatment was determined. We first examined if NAC reduces the production and secretion of IL-1β protein into the medium from macrophages (Fig. 8a). As expected, all inducers elevated IL-1β levels in the medium compared with VC, but co-treatment with NAC significantly reduced the IL-1β levels in all inducer-treated samples. The decrease in IL-1β secretion ranged from 42% for LPS samples to 76% for M-LS and silica samples, with > 60% inhibition for most samples. It has been shown that ROS also interacts with other signaling pathways, such as NF-κB, to regulate the expression of IL-1β (Dinarello 2009). Therefore, NAC may modulate the induction of IL-1β mRNA expression by the inducers. Indeed, cells treated with NAC and fibrogenic inducers had lower IL-1β transcript levels than cells

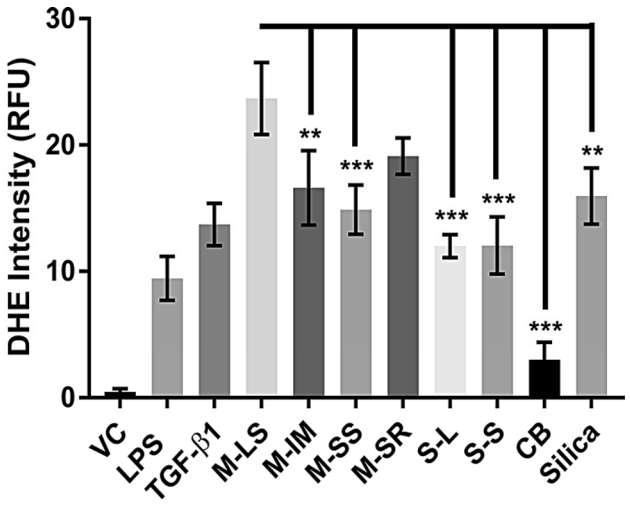

Fig. 7 Treatment with fibrotic inducers causes an increase in ROS levels. Macrophages were treated with fibrogenic inducers and stimulated with ATP as described for Fig. 5. Cells were then fixed and stained using the fluorescent indicator DHE to determine the relative levels of ROS. The relative fluorescent intensity of DHE was quantified. All fibrotic inducers induced a significant increase in ROS levels in macrophages. $^{**}p < 0.01$; $^{***}p < 0.001$

treated with inducers alone, a reduction which reached statistical significance for all treatments except LPS and CB (Fig. 8b). However, the decrease in IL-1β mRNA levels is much less than the decrease in IL-1β protein levels, indicating that NAC may have a bigger inhibition effect on IL-1β protein production and secretion than on IL-1β mRNA expression. In accordance with this, cells treated with NAC showed a significant decrease in NLRP3 activation as measured by ASC speck formation and caspase-1 activity. Therefore, cells co-treated with NAC and inducers had a larger decrease in the formation of ASC specks than cells treated with fibrotic inducers alone (Fig. 8c) with a 50–60% decrease across all treatments. NAC co-treatment also caused a significant decrease in caspase-1 activity levels with inhibition ranging from 55 to 72% for inducer treatments (Fig. 8d). Finally, conditioned media from macrophages treated with both NAC and fibrotic inducers had a significantly blunted effect on fibroblast α-SMA expression and proliferation (Fig. 8e–g), resulting in a 50% or greater reduction in α-SMA expression and staining intensity, and a 30% reduction in the fraction of cells in the G2/M phase, except for CB-treated samples, where the reduction in the percentage of cells in the G2/M phase did not reach statistical significance. Taken together, these results suggest that NLRP3 inflammasome activation by CNTs and silica is ROS-dependent and this ROS-dependent inflammasome activation and subsequent IL-1β release plays a major role in macrophage-guided profibrotic changes for fibroblast activation and proliferation.

Discussion

Pulmonary exposure to some respirable particulates causes fibrosis in the lung characterized by the overgrowth of a collagenous matrix and scarring of lung tissues, which, to a large extent, results from the persistent activation and functioning of myofibroblasts (Dong and Ma 2016b). In these scenarios, myofibroblasts are seemingly continuously differentiated from fibroblasts (and several other types of cells) and have a longer life span than myofibroblasts found in normal wound healing (Hinz et al. 2012). Presumably, multiple signals induced by fibrogenic stimuli elicit and fuel fibroblast differentiation to myofibroblasts in response to a persistent or recurrent fibrogenic stimulus, such as injury, infection, and deposition of foreign bodies, in an inducer, time, and context-dependent manner (Duffield et al. 2013; Wynn and Ramalingam 2012). Identifying such signals and delineating their signaling pathways are highly challenging because of the complexity and the dynamic nature of the interactions among inducers, cells involved, and the matrix that propel fibrosis development. In the current study, we used a conditioned media transfer system to analyze macrophage-guided myofibroblast transformation through secreted factors. In this regard, our study identifies IL-1β as a major mediator that is produced by macrophages exposed to CNTs or silica and stimulates myofibroblast differentiation and activation through media transfer. Moreover, CNTs and silica were shown to elicit robust activation of the NLRP3 inflammasome, which is responsible for the elevated production and secretion of IL-1β. This increase in NLRP3 activation and IL1β secretion is largely diminished by co-treatment with the ROS scavenger NAC in macrophages. These findings support a model in which the ROS-NLRP3 inflammasome-IL-1β axis functions as a predominant pathway to mediate macrophage-initiated fibroblast activation, which may underlie the early phase fibrotic response to particulate deposition in the lung (Fig. 9). Several issues warrant further discussion with respect to the fibrogenic activity and mechanism of action of CNTs and silica.

First of all, this conditioned media transfer approach allows the study of macrophage-fibroblast interactions through secreted cytokines directly, which is fitting for identification of macrophage-generated factors that regulate fibroblast functions during fibrosis development. Importantly, the macrophage responses examined in this model, i.e., elevated IL-1β production, NLRP3 inflammasome activation, ROS production, and myofibroblast transformation (an endpoint response), are robust in both the magnitude of the increase and the percent of cells with a positive response. This robustness enables us to analyze and compare the fibrogenic potentials of a battery of

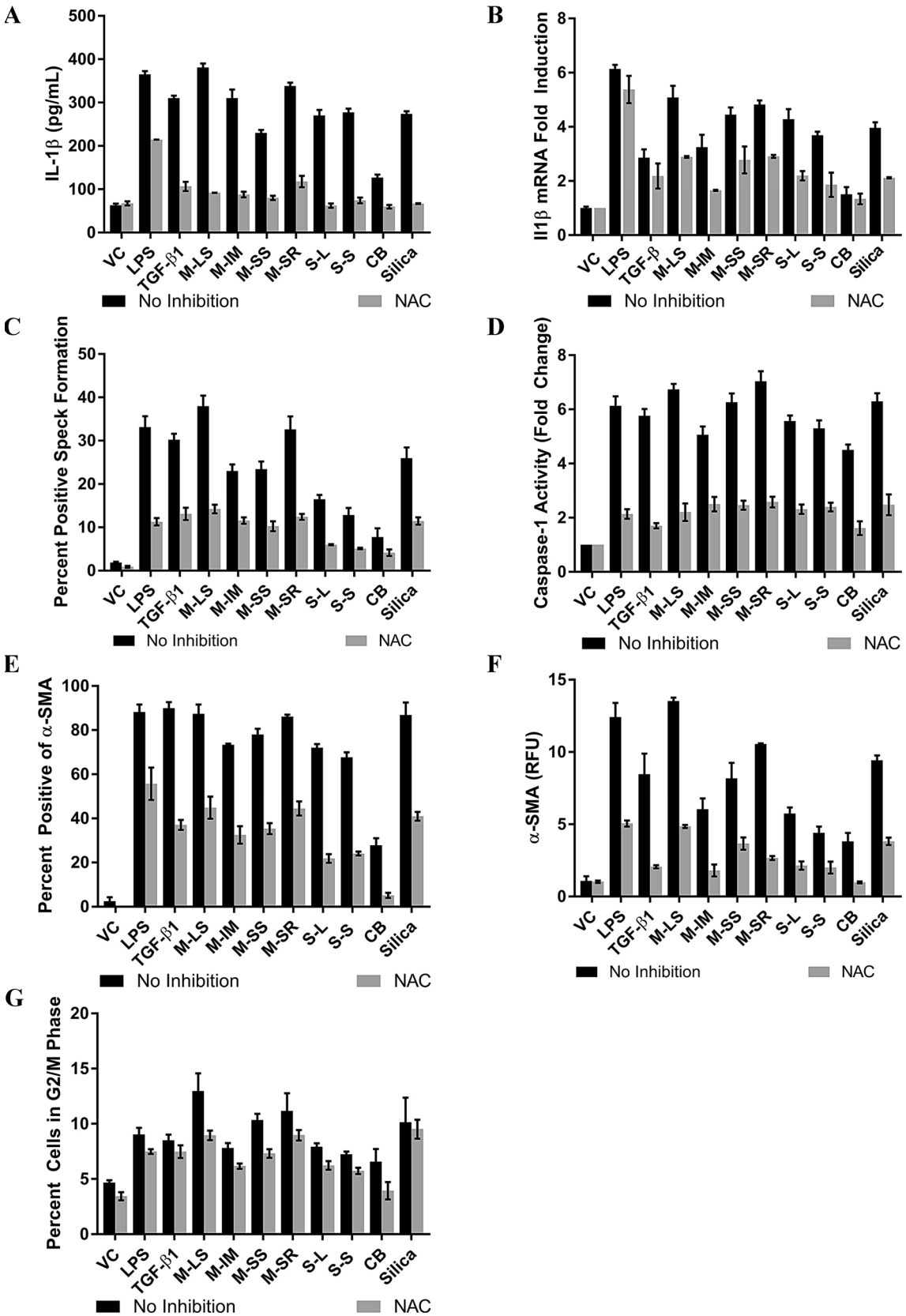
A
IL-1β (pg/mL)
500
400
300
200
100
0
VC
LPS
TGF-β1
M-LS
M-IM
M-SS
M-SR
S-L
S-S
CB
Silica
No Inhibition
NAC
B
Il1β mRNA Fold Induction
8
6
4
2
0
TGF-β
M-IM
C
Percent Positive Speck Formation
50
40
30
20
10
D
Caspase-1 Activity (Fold Change)
E
Percent Positive of α-SMA
100
80
60
40
20
F
α-SMA (RFU)
15
10
5
G
Percent Cells in G2/M Phase

◂**Fig. 8** The ROS scavenger NAC blocks NLRP3 activation in macrophages. **a, b** Macrophages were treated with fibrogenic inducers and 5 mM NAC as described under "Materials and methods". After 24-h treatment, cells were stimulated with ATP and the cells and their conditioned media harvested to measure the levels of secreted IL-1β protein and IL-1β mRNA expression. **c** The activation state of the NLRP3 inflammasome in macrophages co-treated with fibrogenic inducers and NAC was analyzed by ASC speck formation. **d** The caspase-1 activity levels in macrophages treated with fibrogenic inducers and NAC were analyzed. **e–g** The effects of conditioned media from macrophages treated with fibrogenic inducers and NAC on fibroblasts was examined. The addition of NAC significantly reduced the secretion and mRNA expression of IL-1β (**a, b**), as well as the activation of the inflammasome (**c, d**) in macrophages, with exception of mRNA levels in LPS and CB-treated cells, where the reduction did not reach statistical significance. NAC treatment also significantly inhibited the effect of macrophage-conditioned media on fibroblast α-SMA expression and proliferation (**e–g**), excepting TGF-β1 treated cells, where the reduction in cell proliferation did not reach statistical significance

particulate inducers in relation to their physical properties effectively. Our findings support the notion that the pulmonary fibrogenic potentials of CNTs through this ROS-NLRP3 inflammasome-IL-1β axis correlate with the increase in either the length or the diameter of CNTs. The highest activities are those from CNTs with either a very large or very small aspect ratio, i.e., CNTs having a long and slender or a short and rigid shape. Similar conclusions were made in studies that compare different MWCNTs and their pulmonary and pleural effects in various systems (Duke and Bonner 2018; Hamilton et al. 2013; Nagai et al. 2011), including the direct effects of CNTs and silica on fibroblasts (Hindman and Ma 2018). On an equal weight basis, MWCNTs induced higher levels of responses than SWCNTs. While amorphous CB nanoparticles are ineffective in most of the assays, respirable crystalline silica exhibited robust inductive activities that were comparable to those of LPS, TGF-β1, and M-LS and M-SR MWCNTs, which are consistent with the in vivo fibrogenic activities of these inducers.

IL-1β is secreted by macrophages as an acute inflammatory cytokine with multiple functions, including leukocyte chemoattraction, cell proliferation and apoptosis, pyrogenic effect, and inflammatory pain hypersensitivity. IL-1β is elevated in many inflammatory and immune disorders. Therapeutics targeting IL-1β and its receptors are in clinical trial for treating some of these diseases. On the other hand, studies on the role of IL-1β in organ fibrosis have yielded controversial or conflicting results, with some studies showing IL-1β as a potent inducer of fibrosis (Borthwick 2016; Gasse et al. 2007; Liu et al. 2006; Vesey et al. 2002; Wynn and Vannella 2016), and some indicating low or no observable effect, or even anti-fibrotic activity of IL-1β with regard to myofibroblast transformation and fibrosis (Mia et al. 2014). These differences in the effect of IL-1β treatment on fibrotic responses could be due to differences among different testing systems, assays, and treatments (i.e., dose, time, and route of exposure). Few studies have been conducted to examine the role of IL-1β on fibrosis and myofibroblast functions induced by particles and fibers directly. In this regard, several lines of evidence obtained from this study support that IL-1β plays a major role in macrophage-stimulated myofibroblast differentiation and activation in this media transfer model of fibrotic responses. First, IL-1β was highly induced by CNTs and silica at both the protein and mRNA levels. Second, purified IL-1β stimulated robust fibroblast differentiation and proliferation in a concentration-dependent manner. Third, inhibition of IL-1β signaling by an IL-1β-blocking antibody greatly diminished the fibrogenic effects of CNTs and silica. Fourth, co-treatment with other inhibitors, such as MCC950 and NAC, which blocked the fibrogenic effects of these inducers, abolished or strongly inhibited the increased production of IL-1β from activated macrophages. This conclusion of IL-1β as a fibrogenic inducer is consistent with the observation that IL-1β is highly induced during the early acute response to CNTs and silica in the lung that manifests prominent collagen deposition. Therefore, it is rational to posit that macrophage-secreted IL-1β is a major driver of the early phase fibrotic response to fibrogenic particulates, whereas TGF-β1 and IL-13 may have more dominant roles in the acute-to-chronic transition and chronic progression of fibrosis in lungs exposed to particles and fibers as demonstrated previously (Dong and Ma 2016a, 2018a, b; Gieseck et al. 2017).

The production and secretion of IL-1β depends on the activation of the NLRP3 inflammasome, which is a cytoplasmic multiprotein complex that orchestrates innate immune responses to many and diverse stimuli through activation of caspase-1 (Rathinam et al. 2012). Activated caspase-1 cleaves pro-IL-1β and pro-IL-18 to corresponding mature cytokines before they are secreted from macrophages. Activation of the NLRP3 inflammasome requires at least two signals (Jo et al. 2016). Signal 1 or the priming signal is mediated by cytokines, such as TNF-α, or microbial ligands recognized by toll-like receptor (TLR) in the case of microbial infections, both of which activate the NF-κB pathway, leading to the upregulation of pro-IL-1β and NLRP3 gene expression. Signal 2 is mediated by pathogen or damage-associated molecular patterns (PAMPs or DAMPs, respectively), which elicits the oligomerization and complex formation of NLRP3, together with ASC and pro-caspase-1, leading to the cleavage of pro-caspase-1 to functional caspase-1. We have previously shown that MWCNTs activate the NF-κB pathway to increase the transcription of a number of cytokines and chemokines, including TNFα, IL-1β, IL-6, IL-10, and MCP1, in macrophages (He et al. 2011). Therefore, induction of IL-1β transcription serves as a priming mechanism for NLRP3 inflammasome activation by CNTs. NLRP3 can be activated by a variety of

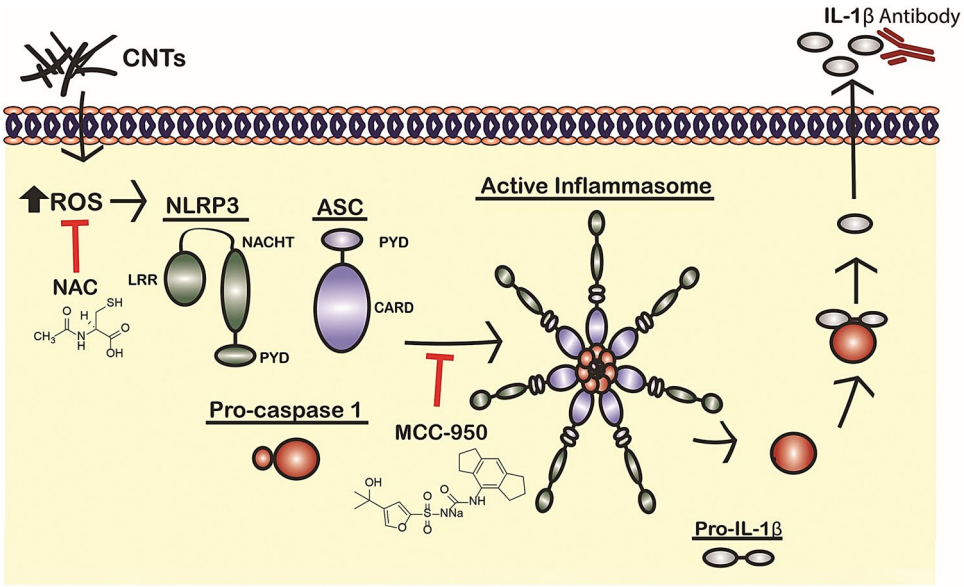

Fig. 9 Proposed mechanism of CNT induced NLRP3 inflammasome activation. Macrophages treated with fibrogenic inducers have an increase in ROS levels within the cell, which activates NLRP3 to associate with ASC and form a large, multi-protein oligomer, or "speck". The close proximity of several copies of pro-caspase-1 within the speck leads to self-cleavage, which activates caspase-1. Activated caspase-1 then cleaves pro-IL-1β to IL-1β, which can then be secreted from the macrophages. Also shown are the inhibitors used in this study: NAC, which scavenges ROS within the cells and thus prevents their effect on NLRP3; MCC-950, which blocks the association of NLRP3 with ASC and thereby prevents speck formation and caspase-1 activation; and IL-1β neutralizing antibody, which binds to and sequesters the IL-1β released by macrophages and blocks its effect on fibroblasts

particulates, including silica, asbestos, cholesterol crystals, and aluminum, and more recently, by nanomaterials such as CNTs (Dostert et al. 2008; Hornung et al. 2008; Palomaki et al. 2011; Yazdi et al. 2010). In this study, we showed a robust activation of the NLRP3 inflammasome by CNTs and silica, evidenced by cytoplasmic speck formation, induced binding between NRLP3 and ACS, elevated caspase-1 activity, elevated level of secreted IL-1β, which correlate with the fibrogenic potential of the inducers. These results indicate that measuring NLRP3 inflammasome activation provides a means of analyzing the relative effects of CNTs in relation to their physical properties effectively, in addition to generating mechanistic insights into the pathogenic effects of particulates.

Although several hypotheses are available regarding NLRP3 inflammasome activation, the initial events of NLRP3 activation remain to be delineated for many, if not all, NLRP3 agonists. This ambiguity is particularly true for the signal 2 of NLRP3 activation by most agonists. Known activators of NLRP3 include potassium flux, lysosomal disruption, calcium signaling, ER stress, and ROS. Notably, increased production of ROS and oxidative stress appear to be a common event that occurs early upon exposure and is required for activation by some NLRP3 agonists (Abderrazak et al. 2015; Elliott and Sutterwala 2015). As discussed above, we have previously shown that MWCNTs activate the NF-κB pathway to up-regulate the transcription of cytokines including IL-1β and this effect correlates with increased production of ROS (He et al. 2011). In this scenario, treatment with MWCNTs caused substantial loss of the electric potential across the inner membrane of the mitochondria, leading to increased ROS production from damaged mitochondria. In this study, we found that CNTs and silica, as well as LPS and TGF-β1, strongly stimulated ROS production, whereas CB induced a minor, albeit significantly higher than the basal level, increase in macrophages. Therefore, elevation of ROS production by the inducers correlates with their ability to activate NLRP3 and induce IL-1β. NAC is a precursor of intracellular cysteine and glutathione. NAC exhibits a strong anti- ROS activity either directly via the redox potential of thiols, or secondarily through increasing glutathione levels in the cells (Halasi et al. 2013; Jiao et al. 2016). Therefore, NAC is used to confirm the involvement of ROS in pathological processes, such as drug-induced apoptosis (Sun 2010). Co-treatment with the ROS scavenger NAC blocked or significantly reduced the induction of IL-1β protein and mRNA, the formation of the NLRP3-ASC speck, and the macrophage-guided myofibroblast transformation. These findings indicate that, not only is the increased ROS production observed in all inducer-treated cells, but also it may be required for both the signal 1 and the signal 2 of NLRP3 inflammasome activation and downstream functions elicited by all inducers tested in this study. Others have also reported increased production of ROS and a potential role

of ROS in NLRP3 activation by various particulates, such as silica, asbestos, and certain nanomaterials, in different experimental systems (Elliott and Sutterwala 2015; Sun et al. 2015; Tschopp and Schroder 2010).

In conclusion, macrophage-guided myofibroblast transformation through conditioned media was used to investigate (a) the relative fibrogenic potentials of CNTs and silica in relation to their physical properties, and (b) the major macrophage-derived soluble factor and its signaling pathway that mediate fibroblast activation and differentiation. CNTs of varying dimensions and respirable crystalline silica, but not nano-sized CB particles, stimulate robust increases in myofibroblast transformation through macrophage-conditioned media. On an equal weight basis, MWCNTs induced higher increases than SWCNTs. Among the MWCNTs tested, those with the largest and the smallest aspect ratios exhibited the highest activities, which were comparable to the activities of LPS, TGF-β1, and silica, thus identifying the length, diameter, and rigidity of CNTs as important parameters for their fibrogenic potentials. The pleiotropic pro-inflammatory cytokine IL-1β was found to be a major cytokine secreted by activated macrophages to drive myofibroblast transformation induced by the inducers through media transfer. Induction of IL-1β requires the NLRP3 inflammasome that is robustly activated by CNTs and silica. The results of this study support a critical role of ROS in NLRP3 activation, IL-1β induction, and macrophage-guided myofibroblast transformation induced by CNTs and silica. In this capacity, ROS may serve as an initial signal for NLRP3 inflammasome activation upon exposure to CNTs and silica.

Funding This work was funded to Q.M. by the Health Effects Laboratory Division and the Nanotechnology Research Center at National Institute for Occupational Safety and Health, Centers for Disease Control and Prevention, USA, No. 8939050W.

Compliance with ethical standards

Conflict of interest The authors declare there are no competing financial interests. The findings and conclusions in this report are those of the authors and do not necessarily represent the official position of the National Institute for Occupational Safety and Health, Centers for Disease Control and Prevention.

References

Abderrazak A, Syrovets T, Couchie D et al (2015) NLRP3 inflammasome: from a danger signal sensor to a regulatory node of oxidative stress and inflammatory diseases. Redox Biol 4:296–307. https://doi.org/10.1016/j.redox.2015.01.008

Birch ME, Ruda-Eberenz TA, Chai M, Andrews R, Hatfield RL (2013) Properties that influence the specific surface areas of carbon nanotubes and nanofibers. Ann Occup Hyg 57(9):1148–1166. https://doi.org/10.1093/annhyg/met042

Borthwick LA (2016) The IL-1 cytokine family and its role in inflammation and fibrosis in the lung. Semin Immunopathol 38(4):517–534. https://doi.org/10.1007/s00281-016-0559-z

Coll RC, Robertson AA, Chae JJ et al (2015) A small-molecule inhibitor of the NLRP3 inflammasome for the treatment of inflammatory diseases. Nat Med 21(3):248–255. https://doi.org/10.1038/nm.3806

de Zoete MR, Palm NW, Zhu S, Flavell RA (2014) Inflammasomes. Cold Spring Harb Perspect Biol 6(12):a016287. https://doi.org/10.1101/cshperspect.a016287

Dinarello CA (2009) Immunological and inflammatory functions of the interleukin-1 family. Annu Rev Immunol 27:519–550. https://doi.org/10.1146/annurev.immunol.021908.132612

Donaldson K, Seaton A (2012) A short history of the toxicology of inhaled particles. Part Fibre Toxicol 9:13. https://doi.org/10.1186/1743-8977-9-13

Donaldson K, Aitken R, Tran L et al (2006) Carbon nanotubes: a review of their properties in relation to pulmonary toxicology and workplace safety. Toxicol Sci 92(1):5–22. https://doi.org/10.1093/toxsci/kfj130

Dong J, Ma Q (2015) Advances in mechanisms and signaling pathways of carbon nanotube toxicity. Nanotoxicology 9(5):658–676. https://doi.org/10.3109/17435390.2015.1009187

Dong J, Ma Q (2016a) In vivo activation of a T helper 2-driven innate immune response in lung fibrosis induced by multi-walled carbon nanotubes. Arch Toxicol 90(9):2231–2248. https://doi.org/10.1007/s00204-016-1711-1

Dong J, Ma Q (2016b) Myofibroblasts and lung fibrosis induced by carbon nanotube exposure. Part Fibre Toxicol 13(1):60. https://doi.org/10.1186/s12989-016-0172-2

Dong J, Ma Q (2016c) Suppression of basal and carbon nanotube-induced oxidative stress, inflammation and fibrosis in mouse lungs by Nrf2. Nanotoxicology 10(6):699–709. https://doi.org/10.3109/17435390.2015.1110758

Dong J, Ma Q (2017a) Osteopontin enhances multi-walled carbon nanotube-triggered lung fibrosis by promoting TGF-beta1 activation and myofibroblast differentiation. Part Fibre Toxicol 14(1):18. https://doi.org/10.1186/s12989-017-0198-0

Dong J, Ma Q (2017b) TIMP1 promotes multi-walled carbon nanotube-induced lung fibrosis by stimulating fibroblast activation and proliferation. Nanotoxicology 11(1):41–51. https://doi.org/10.1080/17435390.2016.1262919

Dong J, Ma Q (2018a) Macrophage polarization and activation at the interface of multi-walled carbon nanotube-induced pulmonary inflammation and fibrosis. Nanotoxicology. https://doi.org/10.1080/17435390.2018.1425501

Dong J, Ma Q (2018b) Type 2 Immune Mechanisms in Carbon Nanotube-Induced Lung Fibrosis. Front Immunol 9:1120. https://doi.org/10.3389/fimmu.2018.01120

Dong J, Porter DW, Batteli LA, Wolfarth MG, Richardson DL, Ma Q (2015) Pathologic and molecular profiling of rapid-onset fibrosis and inflammation induced by multi-walled carbon nanotubes. Arch Toxicol 89(4):621–633. https://doi.org/10.1007/s00204-014-1428-y

Dong J, Yu X, Porter DW, Battelli LA, Kashon ML, Ma Q (2016) Common and distinct mechanisms of induced pulmonary fibrosis by particulate and soluble chemical fibrogenic agents. Arch Toxicol 90(2):385–402. https://doi.org/10.1007/s00204-015-1589-3

Dostert C, Petrilli V, Van Bruggen R, Steele C, Mossman BT, Tschopp J (2008) Innate immune activation through Nalp3 inflammasome sensing of asbestos and silica. Science 320(5876):674–677. https://doi.org/10.1126/science.1156995

Duffield JS, Lupher M, Thannickal VJ, Wynn TA (2013) Host responses in tissue repair and fibrosis. Annu Rev Pathol 8:241–276. https://doi.org/10.1146/annurev-pathol-020712-163930

Duke KS, Bonner JC (2018) Mechanisms of carbon nanotube-induced pulmonary fibrosis: a physicochemical characteristic perspective. Wiley Interdiscip Rev Nanomed Nanobiotechnol 10(3):e1498. https://doi.org/10.1002/wnan.1498

Elliott EI, Sutterwala FS (2015) Initiation and perpetuation of NLRP3 inflammasome activation and assembly. Immunol Rev 265(1):35–52. https://doi.org/10.1111/imr.12286

Fraga D, Meulia T, Fenster S (2008) Real-time PCR. Current protocols essential laboratory techniques. Wiley, p 10.3.1–10.3.33. https://doi.org/10.1002/9780470089941.et1003s0

Gasse P, Mary C, Guenon I et al (2007) IL-1R1/MyD88 signaling and the inflammasome are essential in pulmonary inflammation and fibrosis in mice. J Clin Invest 117(12):3786–3799. https://doi.org/10.1172/JCI32285

Gieseck RL 3rd, Wilson MS, Wynn TA (2017) Type 2 immunity in tissue repair and fibrosis. Nat Rev Immunol. https://doi.org/10.1038/nri.2017.90

Guo H, Callaway JB, Ting JP (2015) Inflammasomes: mechanism of action, role in disease, and therapeutics. Nat Med 21(7):677–687. https://doi.org/10.1038/nm.3893

Halasi M, Wang M, Chavan TS, Gaponenko V, Hay N, Gartel AL (2013) ROS inhibitor *N*-acetyl-L-cysteine antagonizes the activity of proteasome inhibitors. Biochem J 454(2):201–208. https://doi.org/10.1042/BJ20130282

Hamilton RF Jr, Wu Z, Mitra S, Shaw PK, Holian A (2013) Effect of MWCNT size, carboxylation, and purification on in vitro and in vivo toxicity, inflammation and lung pathology. Part Fibre Toxicol 10(1):57. https://doi.org/10.1186/1743-8977-10-57

He X, Ma Q (2012) Redox regulation by nuclear factor erythroid 2-related factor 2: gatekeeping for the basal and diabetes-induced expression of thioredoxin-interacting protein. Mol Pharmacol 82(5):887–897. https://doi.org/10.1124/mol.112.081133

He X, Young SH, Schwegler-Berry D, Chisholm WP, Fernback JE, Ma Q (2011) Multiwalled carbon nanotubes induce a fibrogenic response by stimulating reactive oxygen species production, activating NF-κB signaling, and promoting fibroblast-to-myofibroblast transformation. Chem Res Toxicol 24(12):2237–2248. https://doi.org/10.1021/tx200351d

Hindman B, Ma Q (2018) Carbon nanotubes and crystalline silica induce matrix remodeling and contraction by stimulating myofibroblast transformation in a three-dimensional culture of human pulmonary fibroblasts: role of dimension and rigidity. Arch Toxicol 92(11):3291–3305. https://doi.org/10.1007/s00204-018-2306-9

Hinz B, Phan SH, Thannickal VJ et al (2012) Recent developments in myofibroblast biology: paradigms for connective tissue remodeling. Am J Pathol 180(4):1340–1355. https://doi.org/10.1016/j.ajpath.2012.02.004

Hornung V, Bauernfeind F, Halle A et al (2008) Silica crystals and aluminum salts activate the NALP3 inflammasome through phagosomal destabilization. Nat Immunol 9(8):847–856. https://doi.org/10.1038/ni.1631

Jacobsen NR, White PA, Gingerich J et al (2011) Mutation spectrum in FE1-MUTA(TM) Mouse lung epithelial cells exposed to nanoparticulate carbon black. Environ Mol Mutagen 52(4):331–337. https://doi.org/10.1002/em.20629

Jiao Y, Ma S, Wang Y et al (2016) N-Acetyl cysteine depletes reactive oxygen species and prevents dental monomer-induced intrinsic mitochondrial apoptosis in vitro in human dental pulp cells. PLoS One 11(1):e0147858. https://doi.org/10.1371/journal.pone.0147858

Jo EK, Kim JK, Shin DM, Sasakawa C (2016) Molecular mechanisms regulating NLRP3 inflammasome activation. Cell Mol Immunol 13(2):148–159. https://doi.org/10.1038/cmi.2015.95

Khare S, Radian AD, Dorfleutner A, Stehlik C (2016) Measuring NLR oligomerization I: size exclusion chromatography, co-immunoprecipitation, and cross-linking. Methods Mol Biol 1417:131–143. https://doi.org/10.1007/978-1-4939-3566-6_8

Liu W, Ding I, Chen K et al (2006) Interleukin 1beta (IL1B) signaling is a critical component of radiation-induced skin fibrosis. Radiat Res 165(2):181–191

Mercer RR, Scabilloni JF, Hubbs AF et al (2013) Distribution and fibrotic response following inhalation exposure to multi-walled carbon nanotubes. Part Fibre Toxicol 10:33. https://doi.org/10.1186/1743-8977-10-33

Mia MM, Boersema M, Bank RA (2014) Interleukin-1beta attenuates myofibroblast formation and extracellular matrix production in dermal and lung fibroblasts exposed to transforming growth factor-beta1. PLoS One 9(3):e91559. https://doi.org/10.1371/journal.pone.0091559

Morgan WKC, Seaton A (1995) Occupational lung diseases, 3rd edn. W.B. Saunders Company, Philadelphia

Murray PJ, Wynn TA (2011) Protective and pathogenic functions of macrophage subsets. Nat Rev Immunol 11(11):723–737. https://doi.org/10.1038/nri3073

Nagai H, Okazaki Y, Chew SH et al (2011) Diameter and rigidity of multiwalled carbon nanotubes are critical factors in mesothelial injury and carcinogenesis. Proc Natl Acad Sci USA 108(49):E1330–E1338. https://doi.org/10.1073/pnas.1110013108

NIOSH (2002) Health effects of occupational exposure to respirable crystalline silica. DHHS (NIOSH) Publication No. 2002-129. DHHS CDC NIOSH, Cincinnati

Palomaki J, Valimaki E, Sund J et al (2011) Long, needle-like carbon nanotubes and asbestos activate the NLRP3 inflammasome through a similar mechanism. ACS Nano 5(9):6861–6870. https://doi.org/10.1021/nn200595c

Porter DW, Hubbs AF, Mercer RR et al (2010) Mouse pulmonary dose- and time course-responses induced by exposure to multi-walled carbon nanotubes. Toxicology 269(2–3):136–147. https://doi.org/10.1016/j.tox.2009.10.017

Pozarowski P, Darzynkiewicz Z (2004) Analysis of cell cycle by flow cytometry. Methods Mol Biol 281:301–311. https://doi.org/10.1385/1-59259-811-0:301

Rathinam VA, Vanaja SK, Fitzgerald KA (2012) Regulation of inflammasome signaling. Nat Immunol 13(4):333–342. https://doi.org/10.1038/ni.2237

Sager TM, Castranova V (2009) Surface area of particle administered versus mass in determining the pulmonary toxicity of ultrafine and fine carbon black: comparison to ultrafine titanium dioxide. Part Fibre Toxicol 6:15. https://doi.org/10.1186/1743-8977-6-15

Sargent LM, Porter DW, Staska LM et al (2014) Promotion of lung adenocarcinoma following inhalation exposure to multi-walled carbon nanotubes. Part Fibre Toxicol 11:3. https://doi.org/10.1186/1743-8977-11-3

Sester DP, Zamoshnikova A, Thygesen SJ et al (2016) Assessment of inflammasome formation by flow cytometry. Curr Protoc Immunol 114:14.40.1–14.40.29. https://doi.org/10.1002/cpim.13

Shvedova AA, Kisin ER, Mercer R et al (2005) Unusual inflammatory and fibrogenic pulmonary responses to single-walled carbon nanotubes in mice. Am J Physiol Lung Cell Mol Physiol 289(5):L698–L708. https://doi.org/10.1152/ajplung.00084.2005

Sun SY (2010) Enhancing perifosine's anticancer efficacy by preventing autophagy. Autophagy 6(1):184–185

Sun B, Wang X, Ji Z et al (2015) NADPH oxidase-dependent NLRP3 inflammasome activation and its important role in lung fibrosis by multiwalled carbon nanotubes. Small 11(17):2087–2097. https://doi.org/10.1002/smll.201402859

Suzui M, Futakuchi M, Fukamachi K et al (2016) Multiwalled carbon nanotubes intratracheally instilled into the rat lung induce development of pleural malignant mesothelioma and lung tumors. Cancer Sci 107(7):924–935. https://doi.org/10.1111/cas.12954

Teran FDE (2016) A new approach towards understanding the ion transfer dynamics in nanostructured carbon-based thin films for energy storage applications. Universite Pierre et Marie Curie, Paris

Tomasek JJ, Gabbiani G, Hinz B, Chaponnier C, Brown RA (2002) Myofibroblasts and mechano-regulation of connective tissue remodelling. Nat Rev Mol Cell Biol 3(5):349–363. https://doi.org/10.1038/nrm809

Tschopp J, Schroder K (2010) NLRP3 inflammasome activation: the convergence of multiple signalling pathways on ROS production? Nat Rev Immunol 10(3):210–215. https://doi.org/10.1038/nri2725

Vesey DA, Cheung C, Cuttle L, Endre Z, Gobe G, Johnson DW (2002) Interleukin-1beta stimulates human renal fibroblast proliferation and matrix protein production by means of a transforming growth factor-beta-dependent mechanism. J Lab Clin Med 140(5):342–350. https://doi.org/10.1067/mlc.2002.128468

Wynn TA, Ramalingam TR (2012) Mechanisms of fibrosis: therapeutic translation for fibrotic disease. Nat Med 18(7):1028–1040. https://doi.org/10.1038/nm.2807

Wynn TA, Vannella KM (2016) Macrophages in tissue repair, regeneration, and fibrosis. Immunity 44(3):450–462. https://doi.org/10.1016/j.immuni.2016.02.015

Yazdi AS, Guarda G, Riteau N et al (2010) Nanoparticles activate the NLR pyrin domain containing 3 (Nlrp3) inflammasome and cause pulmonary inflammation through release of IL-1alpha and IL-1beta. Proc Natl Acad Sci USA 107(45):19449–19454. https://doi.org/10.1073/pnas.1008155107

Publisher's Note Springer Nature remains neutral with regard to jurisdictional claims in published maps and institutional affiliations.